

The Role of the Equation of State in Binary Mergers

Saša Ratković

ratkovic@grad.physics.sunysb.edu

*Department of Physics & Astronomy,
State University of New York at Stony Brook,
Stony Brook, NY 11794-3800, USA*

Madappa Prakash

prakash@helios.phy.phiou.edu

*Department of Physics & Astronomy,
Ohio University,
Athens, OH 55701, USA*

James M. Lattimer

lattimer@mail.astro.sunysb.edu

*Department of Physics & Astronomy,
State University of New York at Stony Brook,
Stony Brook, NY 11794-3800, USA*

ABSTRACT

Binary mergers involving black holes and neutron stars have been proposed as major sources of gravitational waves, r-process nucleosynthesis, and gamma ray bursters. In addition, they represent an important, and possibly unique, observable that could distinguish between normal and self-bound neutron stars. These two families of stars have distinctly different mass–radius relationships resulting from their equations of state which can be revealed during their mergers if stable mass transfer ensues. We consider two cases of gravitational-radiation induced binary mergers: (i) a black hole and a normal neutron star, and (ii) a black hole and a self-bound strange quark matter star. We extend previous Newtonian analyses to incorporate the pseudo-general relativistic Paczyński-Wiita potential or a potential correct to second-order post-Newtonian order in Arnowitt–Deser–Misner coordinates. These potentials are employed to study both the orbital evolution of the binary and the Roche lobe geometry that determines when and if stable mass transfer between the components is possible. The Roche lobe geometry with pseudo-general relativistic or post-Newtonian potentials has not heretofore been considered. Our analysis shows that differences in the evolution of normal neutron

stars and strange quark matter stars are significant and could be detected in gravity waves. Both the amplitude and frequencies of the wave pattern are affected. In addition, details of the equation of state for either normal neutron stars or strange quark stars may be learned. A single merger could reveal one or two individual points of the mass-radius relation, and observations of several mergers could map a significant portion of this relation.

Subject headings: dense matter — equation of state — gravitational waves — binaries : close — stars: evolution — stars: neutron

1. Introduction

Mergers of compact objects in binary systems, such as a pair of neutron stars (NS-NS), a neutron star and a black hole (NS-BH), or two black holes (BH-BH), are expected to be prominent sources of gravitational radiation (Thorne 1973). The gravitational-wave signature of such systems is primarily determined by the chirp mass $M_{chirp} = (M_1 M_2)^{3/5} (M_1 + M_2)^{-1/5}$, where M_1 and M_2 are the masses of the coalescing objects. The radiation of gravitational waves removes energy which causes the mutual orbits to decay. For example, the binary pulsar PSR B1913+16 has a merger timescale of about 250 million years, and the pulsar binary PSR J0737-3039 has a merger timescale of about 85 million years (Lyne et al. 2004), so there is ample reason to expect that many such decaying compact binaries exist in the Galaxy. Besides emitting copious amounts of gravitational radiation, binary mergers have been proposed as a source of the r-process elements (Lattimer & Schramm 1976) and the origin of the shorter-duration gamma ray bursters (Eichler et al. 1989).

The expected rates of binary mergers have been estimated by either utilizing the observational information from known binaries or else through theoretical models of binary stellar evolution (population synthesis). The coalescence rate for the NS-NS case has been recently revised upward in view of the newly discovered binary PSR J0737-3039 (Lyne et al. 2004). Due to its low luminosity and relatively short lifetime, the estimated NS-NS merger rate has been increased from prior estimates by almost an order of magnitude (Burgay et al. 2003; Kalogera et al. 2004). The merger rates can be coupled with expected characteristics of future gravity wave detectors to make predictions of the observed merger rate. The updated analysis predicts the observed NS-NS merger rate to be $1.8 \times 10^{-4} \text{ yr}^{-1} \text{ galaxy}^{-1}$ with an uncertainty of about a factor of 3 to 10. For the advanced LIGO detector, it is estimated that mergers up to distances of 350 Mpc (Finn 2001) could be observed, with a total detection rate of up to approximately 1 day^{-1} anticipated (Kalogera et al. 2004). In the NS-BH case the merger rate has been estimated to be about $10^{-5} - 10^{-4} \text{ yr}^{-1} \text{ galaxy}^{-1}$ (Bethe & Brown 1998; Portegies Zwart & Yungelson 1998), or up to 6 times larger than the NS-NS merger rate. It seems likely that this rate might also be adjusted upward by the discovery of PSR J0737-3039.

A neutron star in a binary merger with a larger mass companion will be tidally disrupted. If

the tidal disruption occurs far enough outside the innermost stable circular orbit (ISCO) of the binary, it is expected that an accretion disc will form or that mass transfer to its companion will occur (Clark 1977b; Jaranowski & Krolak 1992; Portegies Zwart 1998). In either case, the gravity wave signal is expected to be significantly different than if tidal disruption occurs after the star penetrates the ISCO. Tidal disruption will occur at larger separations for larger neutron star radii, so some aspects of the neutron star equation of state (EOS) could be determined in the case in which tidal disruption occurs outside the ISCO.

Depending upon the equation of state (EOS) of dense matter and the mass ratio of the binary, tidal disruption could lead to the less massive star overflowing its Roche lobe and transferring its mass through the inner, or first, Lagrange point to its more massive companion. If mass loss from the lighter star occurs quickly enough, and if conservation of mass and orbital angular momentum can be assumed, the two stars will then begin to spiral apart. Although this increases the Roche lobe volume, the radius of the neutron star also increases in response to the mass loss. Mass transfer will continue in a stable fashion if the lighter star can expand sufficiently fast such that it is able to continuously fill its Roche surface. We refer to mass transfer under such conditions as *stable mass transfer*. Because the orbital separation now increases, the gravity wave amplitude will decrease. The signature of stable mass transfer in gravity waves should therefore be strikingly different than for an amorphous tidal disruption or a direct plunge. As we show below, important information about the radius of a neutron star and the underlying equation of state could be contained in the gravity wave signal. The longer timescale produced by stable mass transfer might also extend the duration of an associated gamma ray burst (Portegies Zwart 1998). In the absence of mass transfer, this timescale might be of order milliseconds, the orbital period of the binary near the last stable orbit. In contrast, stable mass transfer extends over a period of at least several tenths of a second.

Another effect of stable mass transfer would be to modify the amount of material potentially ejected from the system. Matter from a tidally disrupted neutron star, which could be accelerated to escape velocities from the binary (Lattimer & Schramm 1976), undergoes decompression which results in heavy nuclei and an intense neutron flux leading to the copious production of r-process elements (Lattimer et al. 1977; Meyer 1989). In the case in which stable mass transfer occurs, sudden disruption of the neutron star near the last stable orbit is avoided, but mass could be transferred unstably at later times and larger separations when the neutron star approaches its minimum stable mass (Colpi et al. 1993).

One of the most significant aspects of the equation of state that stable mass transfer could reveal is whether or not the neutron star is actually a strange quark matter star. It has been suggested that if strange quark matter is the ultimate ground state of matter (i.e., has a lower energy at zero pressure than iron) compression of neutron star matter to sufficiently high density triggers a phase transition which converts virtually the entire neutron star to strange quark matter (Madsen 1999). Such a star is self-bound as opposed to being gravitationally bound as is the case of a normal neutron star.

It has so far proved very difficult to find venues from astrophysical observations that could unambiguously distinguish strange quark stars from normal neutron stars. This is because self-bound stars have similar radii, moments of inertia, and neutrino emissivities and opacities to that of moderate mass normal neutron stars. Therefore, it may be unlikely that photon or neutrino observations, or radio binary pulsar timing measurements, will be able to differentiate these cases, especially if strange quark stars have a small hadronic crust, supported perhaps by electrostatic forces. In that case, the effective temperatures and radii of solar-mass-sized strange quark stars and normal neutron stars would tend to be similar. Even during the proto-neutron star stage, which is observable through neutrino emissions (Burrows & Lattimer 1986), these two types of stellar configurations likely yield similar neutrino signals until such late times that the low luminosities prevent an unambiguous discrimination (Prakash et al. 2000).

However, major differences in the evolutions of normal neutron stars and strange quark matter stars emerge during the final stages of binary mergers if stable mass transfer occurs. These differences would be prominent in both the amplitudes and frequencies of gravitational wave emissions.

The Newtonian equations for orbital motion become progressively inadequate as compact objects spiral inward. For example, the existence and location of the innermost stable circular orbit (ISCO) are not predicted by Newtonian gravitation. Furthermore, in calculations performed to date, the gravitational equipotential surfaces and the size of the Roche lobe have been computed using a Newtonian background (Kopal 1959; Paczyński 1971; Eggleton 1982)). Although a solution in full GR is not yet possible, systematic post-Newtonian corrections have been developed to explore regions close to compact objects (see, for example, (Blanchet 2002)). To extend the Roche lobe overflow model for mass transfer, we will employ recently calculated corrections to the Newtonian results by using the second order post-Newtonian approximation in Arnowitt–Deser–Misner coordinates (Ratković et al. 2005).

We adopt a semi-analytic approach to describe the final stages of NS-NS or BH-NS mergers, extending earlier treatments (Prakash & Lattimer 2003). While the evolution of such mergers has been previously calculated with numerical techniques involving three-dimensional Newtonian hydrodynamics (Kluźniak & Lee 2002), only a few simulations have implemented GR corrections to the orbital evolution or have considered the case in which the inspiralling stars have unequal masses (Davies et al. 2005; Bejger et al. 2005; Shibata et al. 2005; Shibata 2005). In the final phase of a merger, Newtonian orbital mechanics cannot be expected to hold and general-relativistic (GR) corrections become important. In the few cases in which unequal masses were considered, the mass ratios were severely restricted because of numerical difficulties (Shibata et al. 2003).

This work is organized as follows. In §2, we provide the general considerations upon which this work is based on and discuss the mechanism of Roche lobe overflow. The three main ingredients: (1) the evolution of orbital angular momentum, (2) the evolution of the Roche lobe radius, and (3) the EOS parameter that governs these evolutions, are then presented. The differential equations that govern the evolution of the separation distance a and the mass ratio $q = M_1/M_2$ are derived in

this section along with the condition for stable mass transfer. In §3, the EOS’s of normal neutron stars and self-bound quark stars used in this work are summarized. §4 provides the evolution equations for mergers using the second order post–Newtonian potential. We summarize here the recently calculated results for Roche lobes in the second order post–Newtonian approximation (Ratković et al. 2005). In §5, we introduce, in addition to the Newtonian and 2PN analyses, two pseudo–general relativistic potentials for comparisons of binary evolution simulations. We first introduce the potential due to Paczyński & Wiita (1980), and then we modify it to construct a hybrid potential that correctly incorporates some post–Newtonian features. We fit its parameters to match predictions for the position of the innermost stable circular orbit (ISCO) from Blanchet & Iyer (2003), who evaluated the effective gravitational potential up to order $(v^2/c^2)^3$ in post–Newtonian order. We extend the Newtonian analysis of Roche lobes to include the Paczyński–Wiita (Paczyński & Wiita 1980) and hybrid potentials and provide simple fitting results. We consider the corresponding changes to the orbital dynamics that affects the gravitational radiation reaction and the location of the ISCO. Regions of stable mass transfer in the $M_1 - M_2$ plane are identified in §6 for all potentials considered. In §7, we present results of merger simulations for both a normal star and a self-bound star orbiting around another more massive object (BH or NS). A variety of equations of states with varying stiffness at supranuclear density for both cases are considered. Our results pertaining to gravity wave signals are presented in §8. Conclusions are contained in §9.

2. General considerations

Our objective is to explore the role of the EOS as it affects compact binary mergers (see also Lee et al. (2001); Faber et al. (2002); Prakash & Lattimer (2003); Prakash et al. (2004); Shibata et al. (2003); Davies et al. (2005); Bejger et al. (2005); Shibata et al. (2005); Shibata (2005)). In general, a gravitational merger is the result of a system which contains two objects in a mutual orbit decaying via gravitational radiation reaction. When the separation becomes small enough, the less massive object can exceed its Roche lobe and begin to transfer mass to the more massive companion. Typically, this can occur if the mass ratio $q = M_1/M_2$ of the two objects (M_1 is the neutron star mass) is somewhat less than unity. As mass is transferred, the radius of the neutron star readjusts to its new mass on hydrodynamic timescales, which are rapid compared to timescales of orbital evolution. Normally, the radius of a neutron star expands as its mass is lost, but there are exceptions. For example, a self-bound quark star which is not near its maximum mass has a radius which *increases* as the cube root of its mass. But even if this is the case, mass transfer can continue because the Roche lobe radius tends to shrink as q decreases. Even though conservation of angular momentum during mass transfer will reverse the binary’s inspiral, thereby causing an increase in the Roche lobe radius, it is still possible the radius increase can keep pace. If this occurs, the mass transfer is stable. During stable mass transfer, the stellar radius and its Roche lobe remain coincident and mass transfer can continue until the star’s mass becomes very small. For normal neutron stars, stable mass transfer terminates when the star’s mass approaches the minimum neutron star mass of approximately $0.1 M_\odot$, but for strange quark matter stars, it

continues indefinitely.

In our treatment of the star’s orbit, the stars are considered to be point-like masses and the angular momentum of the system is assumed not to be transferred into the spins of the two compact objects. The orbital angular momentum changes only through the emission of gravity waves. We also assume that the total mass of the system is conserved so that mass transfer only exchanges mass between the two bodies and not, for example, into an accretion disc or into material ejected from the system. We do not expect that these assumptions invalidate the qualitative value of our analysis, but adopting a more general treatment might alter some quantitative features such as the gravity wave signal amplitude.

There are four main ingredients in our analysis. First, we assume that mass is conserved during mass transfer. Thus, using $M = M_1 + M_2$,

$$\frac{\dot{M}_1}{M_1} = \frac{1}{1+q} \frac{\dot{q}}{q}. \quad (1)$$

In the case of fixed total mass M , the change of the total angular momentum J depends only on the change of the mass ratio q and the orbital separation a . Second, we assume that the change of J is balanced by the loss of angular momentum J_{GW} that the outgoing gravitational waves carry:

$$\frac{dJ}{dt} = \frac{\partial J}{\partial a} \dot{a} + \frac{\partial J}{\partial q} \dot{q} = -\dot{J}_{GW}. \quad (2)$$

The second ingredient is related to the equipotential surface that regulates mass transfer. The effective sizes of the Roche lobes also depend, for a fixed total mass, only on q and a . Hence, the time dependence of the Roche lobe radius r_{Roche} can be written as

$$\dot{r}_{Roche} = \frac{\partial r_{Roche}}{\partial a} \dot{a} + \frac{\partial r_{Roche}}{\partial q} \dot{q}. \quad (3)$$

The last ingredient incorporates the dependence of binary mergers on the EOS of dense matter. We define a parameter α describing how the radius of the star changes as mass is stripped from it:

$$\alpha(M_1) \equiv \frac{d \ln R_1}{d \ln M_1}. \quad (4)$$

During stable mass transfer the star’s radius remains equal to the Roche radius, that is, $R_1 = r_{Roche}$. We can combine this equality with equations (3) and (4) to establish a connection between the derivatives \dot{a} and \dot{q}

$$\frac{\partial \ln r_{Roche}}{\partial \ln a} \frac{\dot{a}}{a} + \frac{\partial \ln r_{Roche}}{\partial \ln q} \frac{\dot{q}}{q} = \frac{\alpha(M_1)}{1+q} \frac{\dot{q}}{q}, \quad (5)$$

which can be expressed as

$$\frac{\dot{q}}{q} - \Upsilon(a, q) \frac{\dot{a}}{a} = 0, \quad (6)$$

where

$$\Upsilon(a, q) \equiv \frac{\frac{\partial \ln r_{Roche}}{\partial \ln a}}{\frac{\alpha(M_1)}{1+q} - \frac{\partial \ln r_{Roche}}{\partial \ln q}}. \quad (7)$$

We suppress the dependence of variables on the total mass M . Generally, one has $\partial \ln r_{Roche}/\partial \ln a \approx 1$ and $\partial \ln r_{Roche}/\partial \ln q \approx 1/3$. Coupled with the fact that, in general, $\alpha \leq 1/3$ (see §6), one has $\Upsilon(q, a) < 0$.

These results can be combined with equation (2) in order to find the set of coupled differential equations that govern the evolution of a and q . The separation distance evolves in time according to

$$\dot{a} = - \frac{\dot{J}_{GW}(a, q)}{\frac{\partial J(a, q)}{\partial a} + \Upsilon(a, q) \frac{q}{a} \frac{\partial J(a, q)}{\partial q}}, \quad (8)$$

and simultaneously the mass ratio changes according to

$$\dot{q} = - \frac{\dot{J}_{GW}(a, q) \Upsilon(a, q)}{\frac{a}{q} \frac{\partial J(a, q)}{\partial a} + \Upsilon(a, q) \frac{\partial J(a, q)}{\partial q}}. \quad (9)$$

In stable mass transfer, M_1 decreases so q does also. Furthermore, it is generally true that $\partial J/\partial a > 0$ and $\partial J/\partial q > 0$. Thus, the condition for stable mass transfer is simply

$$\Upsilon(a, q) > - \frac{\partial \ln J(a, q)/\partial \ln a}{\partial \ln J(a, q)/\partial \ln q}. \quad (10)$$

During stable mass transfer, $\dot{a} > 0$ and, hence, the binary spirals apart. However, if this condition is subsequently violated, mass transfer either ceases or becomes unstable. If mass transfer terminates, emission of gravitational radiation leads to a contraction of the orbit, whereupon mass transfer may be able to begin again. In either case, this limit spells a quick end to the star.

Equations (8) and (9) determine the time evolution of a and q . From these quantities, all other relevant quantities can be determined during mass transfer. The details will depend upon the EOS and upon the gravitational potential assumed. In the following sections, we explore several gravitational potentials and corresponding models for the Roche radius to study the behavior of binary systems that are built of stars with different equations of state.

We anticipate that tidal distortions, which give rise to the Roche geometry, do not significantly alter the orbital evolution, because the associated gravitational radiation corrections are small (see Chau (1976) and Clark (1977a)). We also restrict ourselves to the study of conservative mass transfer (in which angular momentum is conserved).

3. The equation of state

Several proposals concerning the physical state and the internal constitution of matter at supra-nuclear densities have been put forth (see Lattimer & Prakash (2001); Alford (2001) for recent accounts). The many exciting possibilities for the composition of compact stars include (1) strangeness-bearing matter in the form of hyperons, kaons, or quarks, (2) Bose (pion or kaon) condensed matter, and (3) so-called self-bound strange quark matter (SQM). Fermions, whether they are in the form of baryons or deconfined quarks, are expected to additionally exhibit superfluidity and/or superconductivity. The possibility of such exotic phases brings attendant changes to the predictions of maximum masses and radii, since the presence of multiple components or new phases of matter generally lessens the pressure for a given energy density. For the discussion at hand, we will use the term normal star to refer to a star with a surface of normal matter in which the pressure vanishes at vanishing baryon density. The interior of the star, however, may contain any or a combination of the above exotica.

A self-bound star is exemplified by Witten’s SQM star (Witten 1984); see Alcock & Olinto (1988) for a review. Such a star has a bare quark matter surface in which the pressure vanishes at a finite but supra-nuclear baryon density. In the context of the MIT bag model with first order corrections due to gluon exchange, the baryon density at which pressure vanishes is

$$n_b(P = 0) = (4B/3\pi^{2/3})^{3/4}(1 - 2\alpha_c/\pi)^{1/4}, \quad (11)$$

where B is the bag constant and $\alpha_c = g_c^2/(4\pi)$ is the quark-gluon coupling constant. This density is not significantly affected by the finite strange quark mass (Prakash et al. 1990) or by the pairing phenomenon in quark matter (Madsen 2002).

Prototypes of the radius versus mass for broadly differing EOS’s selected from Lattimer & Prakash (2001) are shown in Figure 1. Table 1 summarizes the nomenclature used in this figure as well as the masses and radii of the maximum configurations of stars constructed using these EOS’s. Quantitative variations from these generic behaviors can be caused by uncertainties in the underlying strong interaction models (see the compendium of results in Figure 2 of Lattimer & Prakash (2001)). Qualitative differences in the outcomes of mergers with a black hole emerge, however, because of the gross differences in the mass-radius diagram.

A normal star and a self-bound star represent two quite different possibilities (see the right panel in Figure 1) for the quantity

$$\alpha \equiv \frac{d \ln R}{d \ln M} \begin{cases} \leq 0 & \text{for a normal neutron star (NS)} \\ \geq 0 & \text{for a self-bound SQM star} \end{cases}, \quad (12)$$

where M and R are the star’s mass and radius, respectively. For small to moderate mass self-bound stars, $R \propto M^{1/3}$ so that $\alpha \cong 1/3$; only for configurations approaching the maximum mass does α turn negative.

Table 1. EQUATIONS OF STATE

Symbol	Approach	Composition	$M_{max}[M_{\odot}]$	$R(M_{max})$ [km]
AP4 ^a	Variational	np	2.21	10.0
MS0 ^b	Field Theoretical	np	2.77	13.32
PAL6 ^c	Schematic Potential	np	1.48	9.23
GS1 ^d	Field Theoretical	npK	1.38	8.27
SQM1 (SQM3) ^e	Quark Matter	Q (u, d, s)	1.56 (1.93)	8.54 (10.69)

Note. — Approach refers to the underlying theoretical technique. Composition refers to strongly interacting components (n=neutron, p=proton, H=hyperon, K=kaon, Q=quark); all models include leptonic contributions. The last two columns contain the corresponding masses and radii of the maximum mass configurations.

^aAkmal & Pandharipande (1997)

^bMüller & Serot (1996)

^cPrakash, Ainsworth & Lattimer (1988)

^dGlendenning & Schaffner-Bielich (1999)

^ePrakash, Cooke & Lattimer (1995)

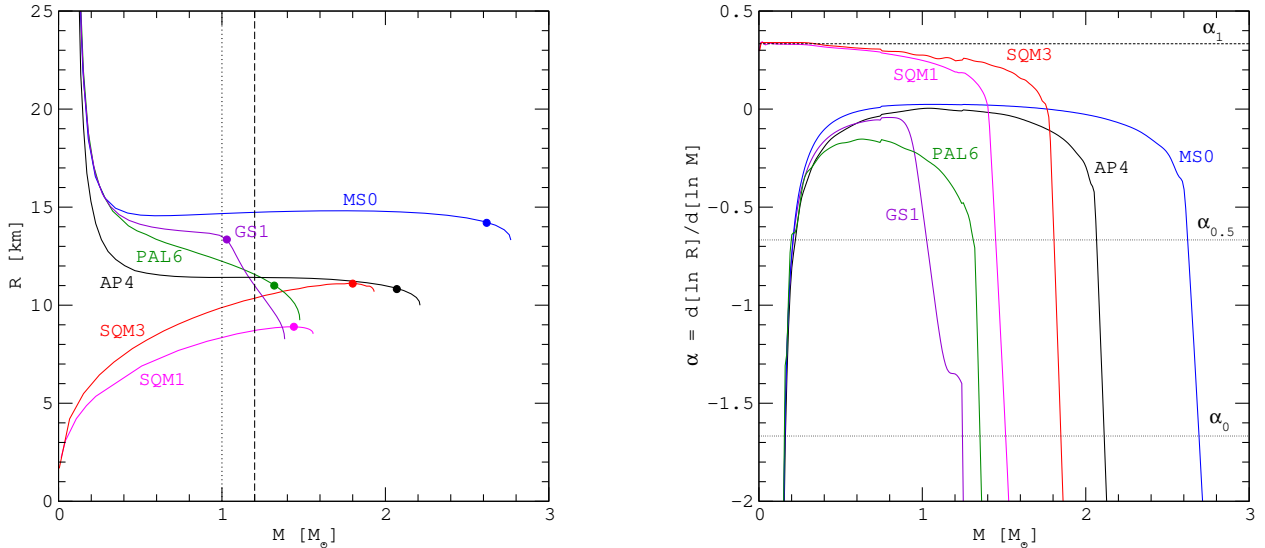


Fig. 1.— Radius versus mass (left panel) and its logarithmic derivative (right panel) for prototype EOS’s. The EOS symbols are as in Lattimer & Prakash (2001). The vertical lines in the left panel and the horizontal lines in the right panel are discussed in §6. In the left panel, the maximum masses for which stable mass transfer is allowed in the case $q = 0.5$ are denoted by filled circles for each EOS.

Our objective is to explore the astrophysical consequences of these distinctive behaviors in R versus M as they affect mergers with a black hole. Note that α is intimately connected with the dense matter equation of state (EOS), since there exists a one-to-one correspondence between $R(M)$ and $P(n_B)$, where P is the pressure and n_B is the baryon density. Gravitational mergers in which a compact star loses its mass (either to a companion star or to an accretion disk) during evolution is one of the rare examples in which the R versus M (or equivalently, P versus n_B) relationship of the same star is sampled. Although we focus here on the coalescence of a compact star with a BH, the theoretical formalism and our principal findings apply also to mergers in which both objects are compact stars.

4. Mergers with the second order post-Newtonian potential

Under moderately strong gravitational fields, the post-Newtonian approximation has been widely used to study systems in which general relativistic corrections are considered to be important. Ratković et al. (2005) have recently calculated corrections to the Newtonian results for the Roche lobe geometry by using the second order post-Newtonian approximation in the Arnowitt–Deser–Misner coordinates. Starting from the N-body Lagrangian derived by Damour & Schäfer (1985), Ratković et al. (2005) developed the Lagrangian for a test particle in the vicinity of two massive

compact objects. This calculation required the use of an approximate expression for the transverse–traceless term U_{TT} of the Lagrangian, since an exact result is not available. The approximate form for U_{TT} that is valid in the vicinity of the less massive star was established. Next, the 2PN effective potential in the co–rotating frame was found and in a similar fashion as for the Newtonian case, the resulting values of the effective Roche lobe radius as functions of q and a could be determined. Technically, the post-Newtonian Roche radii can be adequately parametrized by the quantities q , a , and the relativity parameter $z = 2M/a$, the dimensionless ratio of the effective event horizon of the total mass and the semi-major axis. In the case in which the total mass M is assumed conserved, z varies inversely with a . The results can thus be presented in a form that closely resembles Newtonian expressions that depend only upon a and q .

4.1. Analytic fits to Roche lobe radii to 2 PN

In Newtonian gravity, the potential surfaces are proportional to a and otherwise a function of only the mass ratio q , and are to a sufficient accuracy often described by the Eggleton approximation (Eggleton 1982):

$$\frac{r_{Roche}}{a} = Q(q) \equiv \frac{\alpha_Q q^{2/3}}{\beta_Q q^{2/3} + \ln(1 + q^{1/3})}, \quad (13)$$

with $\alpha_Q = 0.49$ and $\beta_Q = 0.57$ as parameters. Here, r_{Roche} is the radius of a sphere of the same volume $V_{Roche} = 4\pi r_{Roche}^3/3$ of the equipotential surface which extends through the first, or inner, Lagrangian point. We will assume that Roche lobe overflow occurs when the radius of the star R_1 exceeds the effective Roche radius r_{Roche} , even though the true equipotential surface is not spherical. We will also assume that tidal deformations of the stars do not affect the Roche picture of mass transfer significantly.

To extend the Newtonian treatment to the post-Newtonian case, an adequate approximation was constructed by Ratković et al. (2005) by utilizing an additional relativity parameter $z = 2M/a$ corresponding to the ratio of the effective event horizon of the total mass and the orbital separation:

$$\frac{r_{Roche}}{a} = Q(q)C(q, z), \quad (14)$$

where

$$C(q, z) = 1 + z(\alpha_C q^{1/5} - \beta_C) \quad (15)$$

with $\alpha_C = 1.951$ and $\beta_C = 1.812$. We emphasize that the z dependence is equivalent to an a dependence when M is constant. The Roche equipotential surfaces (which all scale with the orbital separation a) in the equatorial plane along a line through the stars’ centers of mass are displayed in Figure 2 for a variety of q and z values. The results for the Roche lobe radii, and the fits we adopted from Ratković et al. (2005), are shown in Figure 3. Note the common point $q = (\beta_C/\alpha_C)^5 \simeq 0.69$ in these results.

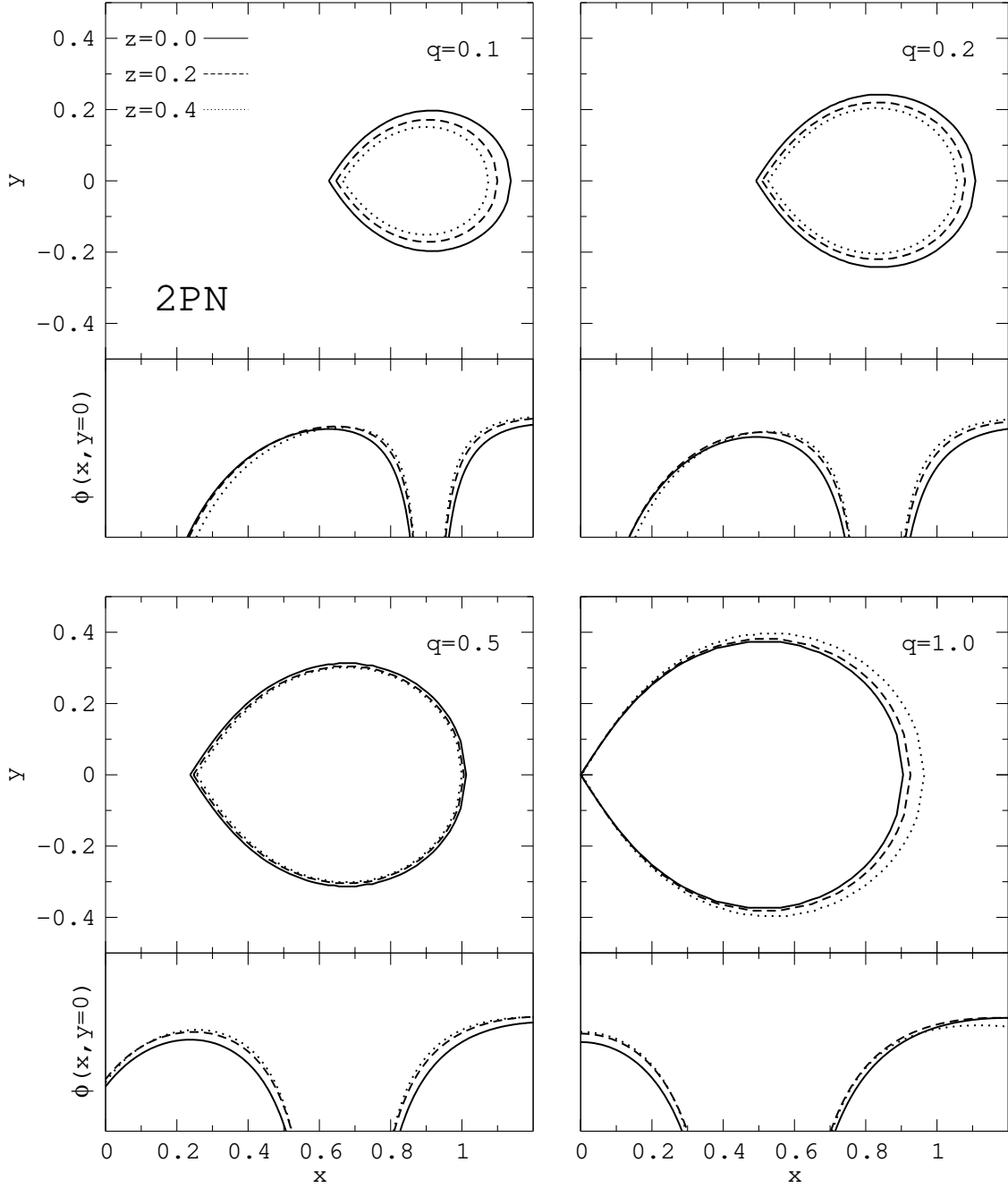


Fig. 2.— Roche lobes and the corresponding potentials for $y = 0$ for the second order post-Newtonian (2PN) potential. Coordinates x and y are scaled by the stellar separation a and are shown for $q = 0.1, 0.2, 0.5,$ and $1.0,$ respectively. Results are shown for values of $z = 0, z = 0.2,$ and $z = 0.4,$ respectively.

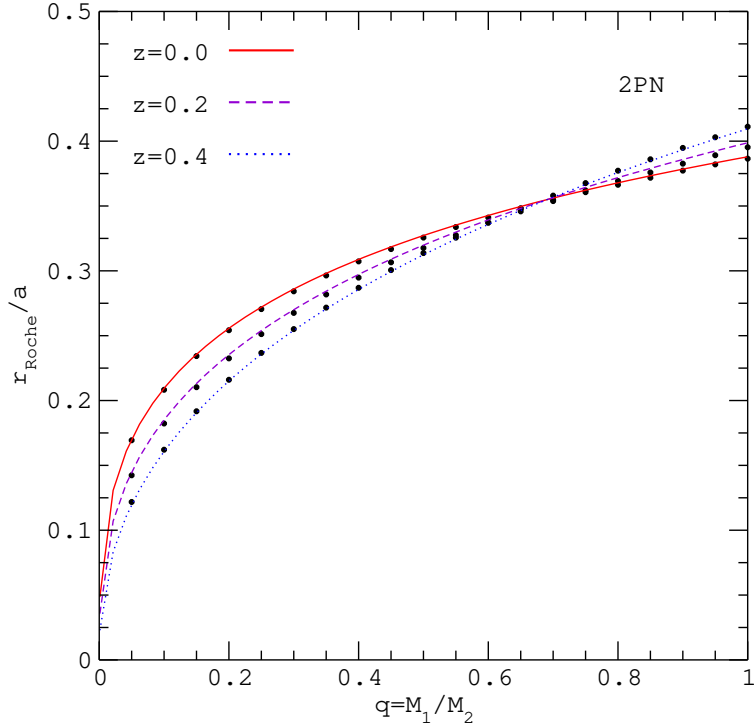


Fig. 3.— Effective Roche lobe radii r_{Roche} for the 2PN potential scaled by the stellar separation a versus mass ratio q for $z = 0$, $z = 0.2$, and $z = 0.4$, respectively.

4.2. Evolution equations

In order to model the orbital evolution of the merging stars, it is necessary to develop an appropriate expression for the orbital angular momentum J . Although the angular momentum in the ADM approximation has been derived up to the 3PN order (de Andrade et al. 2001; Blanchet & Iyer 2003)), for consistency we use results up to the 2PN level. For quasi-circular motion, the angular momentum is

$$J = \sqrt{a}M^{3/2} \frac{q}{(1+q)^2} \left\{ 1 + 2 \frac{M}{a} - \frac{1}{16} \frac{48 + 79q + 104q^2 + 79q^3 + 48q^4}{(1+q)^4} \left(\frac{M}{a} \right)^2 \right\}, \quad (16)$$

where $M = m_1 + m_2$. The post-Newtonian correction is given by the second and third terms. Under the assumption of conserved total mass, the angular momentum is only a function of a and q even in this case. The angular momentum loss due to gravitational wave emission (see equation (4.9) and related discussion in Blanchet & Iyer (2003)) is, in the same approximation,

$$\frac{dJ}{dt} = \frac{\partial J}{\partial a} \dot{a} + \frac{\partial J}{\partial q} \dot{q} = -\dot{J}_{GW} = -\frac{32}{5} \frac{q^2}{(1+q)^4} \frac{M^{3/2}}{a^{1/2}} \left(\frac{M}{a} \right)^3 + \mathcal{O} \left[\left(\frac{M}{a} \right)^4 \right], \quad (17)$$

where the $\mathcal{O}\left(\left(\frac{M}{a}\right)^4\right)$ terms will be neglected. The partial derivatives with respect to a and q in equation (16) are

$$\frac{\partial J}{\partial a} = \frac{1}{2} \frac{M^{3/2}}{a^{1/2}} \frac{q}{(1+q)^2} \left\{ 1 - 2\frac{M}{a} + \frac{1}{16} \left(\frac{M}{a}\right)^2 \frac{144 + 237q + 312q^2 + 237q^3 + 144q^4}{(1+q)^4} \right\}, \quad (18)$$

and

$$\frac{\partial J}{\partial q} = a^{1/2} M^{3/2} \frac{1-q}{(1+q)^3} \left\{ 1 + 2\frac{M}{a} + \frac{1}{8} \left(\frac{M}{a}\right)^2 \frac{-3 + 101q + 145q^2 + 101q^3 - 3q^4}{(1+q)^4} \right\}. \quad (19)$$

We are now equipped to investigate for what choices of masses M_1 and M_2 (i) stable mass transfer will occur, and (ii) whether mass transfer will begin before the ISCO is reached. Before performing this analysis, however, we investigate two alternative approaches to extending the Newtonian analysis to the relativistic regime. Neither of these alternate models have been fully explored with the semi-analytic approach we will utilize for the 2PN methodology described above, so we do this in the next section.

5. Mergers with pseudo-GR potentials

As a simple alternative analysis that can be easily tailored to fit some aspects of GR, the Paczyński–Wiita potential (Paczyński & Wiita 1980) was used by Kluźniak & Lee (2002). In our work, to mimic the GR effects, we also use this family of pseudo-potentials which replace the Newtonian potential $\phi_N(r) = -M/r$. We endeavor that pseudo-GR potentials accurately predict the existence of the ISCO for the general case. The Paczyński–Wiita potential correctly predicts its location for the case of two arbitrary point masses. We introduce an improved form of this potential, the hybrid pseudo-general relativistic (henceforth pseudo-GR) potential, in order to fit this potential more closely to post-Newtonian results in the case of two noninfinitesimal masses.

5.1. Paczyński–Wiita potential

Pseudo-potentials have proved useful for incorporating general relativistic effects in the study of accretion disks surrounding a massive central body. For test particles near a highly relativistic object, Paczyński & Wiita (1980) introduced a pseudo-GR potential which we will refer to as the PW potential:

$$\phi_{PW}(r) = -\frac{M_2}{r - r_{G2}}, \quad (20)$$

where M_2 is the mass of the central compact object, r is the distance to the center of this object, and $r_{G2} = 2M_2$ is its Schwarzschild radius. Applied to a test particle, this potential both mimics the existence of an event horizon at $r = r_{G2}$ and correctly predicts that the ISCO is at $r = 3r_{G2}$. For other examples of pseudo-potentials, see Lee et al. (2001).

5.2. Hybrid pseudo-GR potential

The location of the ISCO for the PW potential agrees with the GR result only for an orbiting particle with negligible mass. However, with slight modification, the point of gravitational instability of the Paczyński–Wiita potential can be positioned at the desired radius. For a binary consisting of two nearly equal masses, post-Newtonian results (Blanchet & Iyer 2003) valid up to 3PN order predict that the ISCO moves inward compared to the point-particle result ($3r_G$). We can simulate these results by minimally modifying the PW potential. Explicitly, we adopt the hybrid potential

$$\phi_H(r) = -\frac{M}{r - \zeta(q)r_G}, \quad (21)$$

where $M = M_1 + M_2$ is the total mass, $r_G = 2M$ is the sum of the horizon radii of the two stars, and the function $\zeta(q) \in (0, 1)$ contains the necessary corrections to account for the position of the ISCO as a function of the mass ratio $q = M_1/M_2$ of the two components. We take M_1 to be the less massive star, so that $q < 1$. In the case of a test particle, the function $\zeta(0) = 1$, whereas for finite M_1 , the correction function $\zeta(0 \leq q \leq 1) < 1$. With this hybrid potential, the orbital separation corresponding to the ISCO becomes

$$r_{ISCO} = 3\zeta(q)r_G. \quad (22)$$

We require that the hybrid potential predict the ISCO as closely as possible to post-Newtonian results up to third order. As shown by Blanchet & Iyer (2003), the ISCO radius at which the gravitational instability occurs for a binary system with a mass ratio q can be found in the 3PN approximation by solving the cubic equation resulting from extremizing the gravitational potential,

$$1 + \alpha(\nu)x + \beta(\nu)x^2 + \gamma(\nu)x^3 = 0 \quad (23)$$

with coefficients

$$\begin{aligned} \alpha(\nu) &= -9 + \nu, & \beta(\nu) &= \frac{117}{4} + \frac{43}{8}\nu + \nu^2, & \text{and} \\ \gamma(\nu) &= -61 + \left(\frac{135403}{1680} - \frac{325}{64}\pi^2 - \frac{99}{3}\lambda \right) \nu - \frac{31}{8}\nu^2 + \nu^3, \end{aligned} \quad (24)$$

where $\nu = q/(1+q)^2$. The quantity λ arises from considerations of dimensional regularization, and following Blanchet & Iyer (2003), we set $\lambda = 0.64$. The ISCO radius is then $r_{ISCO} = M/x_0(\nu)$, where $x_0(\nu)$ denotes the solution of the cubic equation 23. We find that the 3PN corrections can be fitted by a function ζ_{FIT} that is a third order polynomial in q

$$\zeta_{FIT}(q) = 0.697 + 0.214(1.07 - q)^3. \quad (25)$$

The radius of the ISCO r_{ISCO} to order 3PN, the correction function $\zeta(q)$, and the fitted correction function $\zeta_{FIT}(q)$ are shown in Figure 4. We note that $\zeta_{FIT}(q)$ does not perfectly reproduce the general relativistic result (*i.e.*, $\zeta(0) = 1$) in the limit of small q . This is a consequence of the slow convergence of the post-Newtonian approach, which is here truncated at the 3PN order.

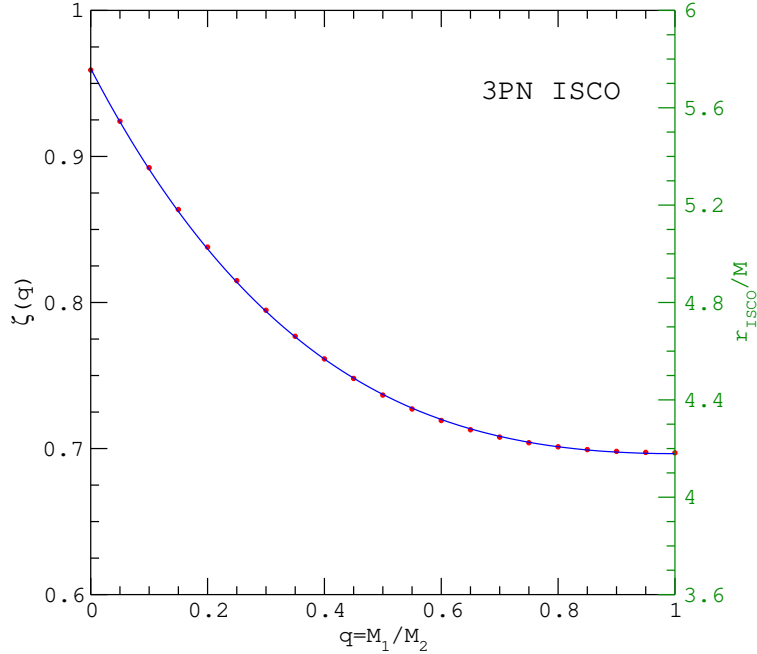


Fig. 4.— The ISCO radius and the correction function $\zeta(q)$ given by 3PN results. The correction function $\zeta(q)$ as determined by solving the cubic equation (23) are shown as dots while the fitted function given by equation (25) is represented by the solid line.

5.3. Roche lobe radii with analytical fits

Differences between the Paczyński–Wiita potential and the hybrid potential predictions for Roche lobe radii are minimal. The Paczyński–Wiita results can be obtained by setting $\zeta(q) = 1$ in the expressions utilized for the hybrid potential. Hence, we establish expressions for the hybrid case only.

Beginning from the hybrid pseudo-GR potential ϕ_H in equation (21) that describes the orbital evolution, we assume that the same potential describes the motion of test particles in the vicinity of two orbiting massive objects in general relativity. We establish equipotential surfaces using the same methodology as Kopal (1959), Paczyński (1971), and Eggleton (1982), who studied the Newtonian Roche geometry. In the potential ϕ_H , the motion of either mass M_i with position vector \vec{r}_i in the co-rotating frame is governed by

$$M_i \left(\frac{d^2 \vec{r}_i}{dt^2} \right)_{rot} = M_i \left(\frac{d^2 \vec{r}_i}{dt^2} \right)_{inertial} - M_i \vec{\omega} \times (\vec{\omega} \times \vec{r}_i) \quad (26)$$

where $i = 1, 2$. The force on either body in the inertial frame is given by the gravitational attraction of the potential in equation (21). Setting the acceleration in the rotating frame to zero, the angular

frequency of the binary, using the potential ϕ_H , is given by

$$\omega^2 = \frac{M}{a[a - \zeta(q)r_G]^2}, \quad (27)$$

where $a = |\vec{r}_1 - \vec{r}_2|$ is the distance between them. The Newtonian result $\omega^2 = M/a^3$ obtains in the limit $r_G/a \rightarrow 0$. In a similar fashion, the position \vec{r} of a third body, with mass m negligible compared to the two large masses M_1 and M_2 , in the corotating frame is governed by

$$\left(\frac{d^2\vec{r}}{dt^2}\right)_{rot} = \left(\frac{d^2\vec{r}}{dt^2}\right)_{inertial} - \vec{\omega} \times (\vec{\omega} \times \vec{r}) - 2\vec{\omega} \times \frac{d\vec{r}}{dt}. \quad (28)$$

The right hand side includes both the centrifugal force and the Coriolis force. Inserting the acceleration using the hybrid potential in equation (21) in equation (28) and integrating, the effective potential in the rotating frame is given by

$$\phi_H^{rot}(x, y) = -\frac{M}{a} \left[\frac{x_2}{\sqrt{(x+x_1)^2 + y^2} - x_2 z} + \frac{x_1}{\sqrt{(x-x_2)^2 + y^2} - x_1 z} + \frac{1}{2} \frac{x^2 + y^2}{(1 - \zeta(q)z)^2} \right], \quad (29)$$

where we have introduced the dimensionless variables

$$\begin{aligned} x &= \frac{r_x}{a}, & y &= \frac{r_y}{a}, & z &= \frac{r_G}{a} = 2\frac{M}{a} \\ x_1 &= \frac{M_2}{M} = \frac{1}{1+q} & x_2 &= \frac{M_1}{M} = qx_1. \end{aligned} \quad (30)$$

Note that x_1 (x_2) denotes the position of the mass M_1 (M_2) on the negative (positive) dimensionless x-axis. z is a relativity parameter. In writing the above equation, we used the facts that $\zeta(m/M_1) \rightarrow 1$ and $\zeta(m/M_2) \rightarrow 1$ for the negligible mass m of the test particle. Note that the effects of the test particle on the total gravitational potential and on the orbital angular frequency ω are taken to be negligible.

By using equation (29), it is now possible to find the Roche lobes for the Paczyński–Wiita and for the hybrid cases. Figures 5 and 6 display contours of the effective potentials $\phi_{PW}^{rot}(x, y)$ and $\phi_H^{rot}(x, y)$, and its Roche lobes for four values of q and three values of z . In contrast to the Newtonian case, for which the Roche lobe radii depend only on the parameter q , the Roche lobe radii for the two pseudo-potentials depend on the additional dimensionless parameter $z = r_G/a$.

For finite z , the hybrid potential in equation (21) causes an effective increase in the strength of gravity compared to the Newtonian case. This decreases the value of the potential at the inner Lagrange point L_1 for all values of q . For every q , the inner Lagrangian point moves closer to the lighter mass as z increases. For a given value of q , the volume contained within the equipotential surface defined by the value of the potential at L_1 , i.e., the Roche lobe volume, changes monotonically with z . For $q < (\beta_C/\alpha_C)^5$, which is 0.63 (0.39) in the case of the hybrid (Paczyński–Witta) potential, the Roche lobe volume decreases with increasing relativity parameter z . The opposite behavior is found for larger values of q .

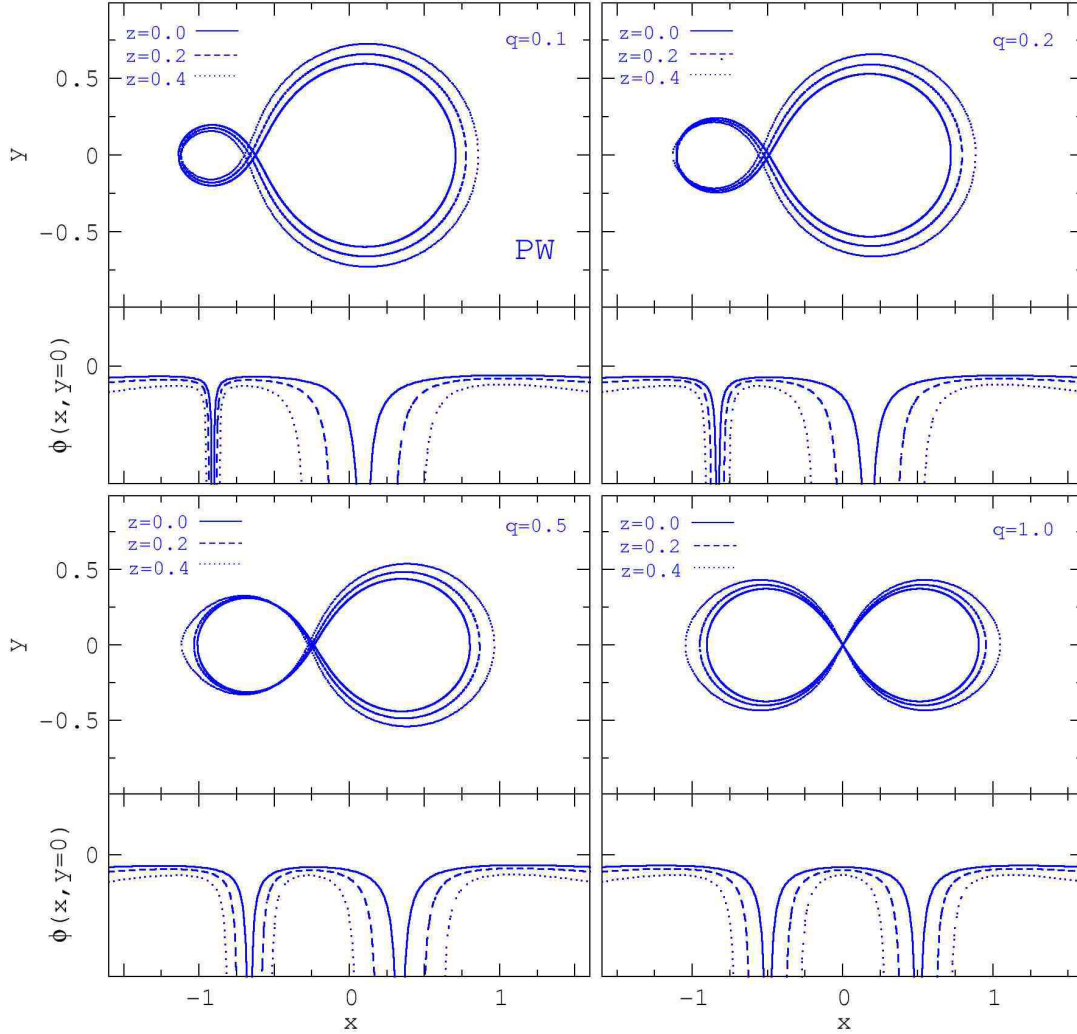


Fig. 5.— Dependence of the Paczyński-Wiita potential and its Roche lobes on q and z .

After performing numerical integration of the Roche lobes we find that the Roche lobe radii for both potentials can be adequately described by using the same functional form as in equation (14) with $Q(q)$ given by equation (13); the parameters α_C and β_C for the hybrid and for the PW potentials are listed in Table 2. For comparison, parameters for the 2PN potential are also given in this table. Numerical determinations of the Roche lobe radii are compared with these fits in Figures 7 and 8. The case $z = 0$ corresponds to the Newtonian case studied by Eggleton (1982).

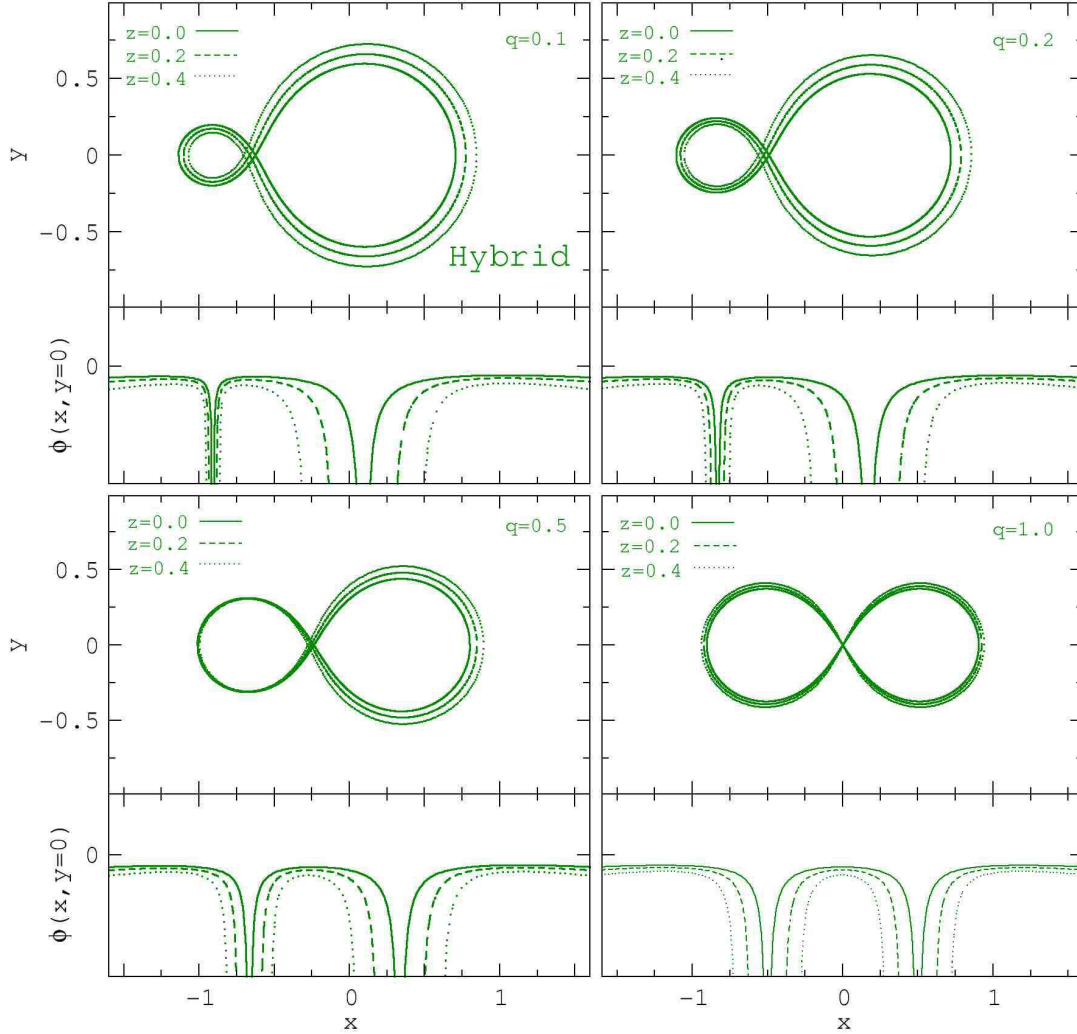


Fig. 6.— Dependence of the hybrid pseudo-GR potential and its Roche lobes on q and z .

These calculations are restricted to values of z limited by the condition that the ISCO radius remains smaller than the separation distance. Quantitatively, this condition amounts to $z < \zeta(q)^{-1}/3 \simeq 0.33 - 0.5$. Secondly, for large z and small q , the inner Lagrange point L_1 becomes the global extremum of the potential. Consequently, the stars cannot remain in contact and mass overflow from the lighter star does not flow through L_1 to the other star. In such a situation, the Roche lobe analysis cannot be used to describe mass transfer. Therefore, we restrict ourselves

Potential	α_C	β_C
Paczyński–Wiita	2.398	1.988
Hybrid	2.328	2.122
2PN	1.951	1.812

Table 2: Values for the fitting parameters in equation (15) for the potentials that are used in sections 5 and 7 for modeling binary evolution with mass transfer. The fitting results for the Paczyński–Wiita and the hybrid pseudo-GR potentials are depicted in Figures 7 and 8, whereas the second order post–Newtonian results are taken from Ratković et al. (2005).

to $0 \leq z \leq 0.5$. We also note that the hybrid potential becomes unreliable for large z as it lacks the full content of GR.

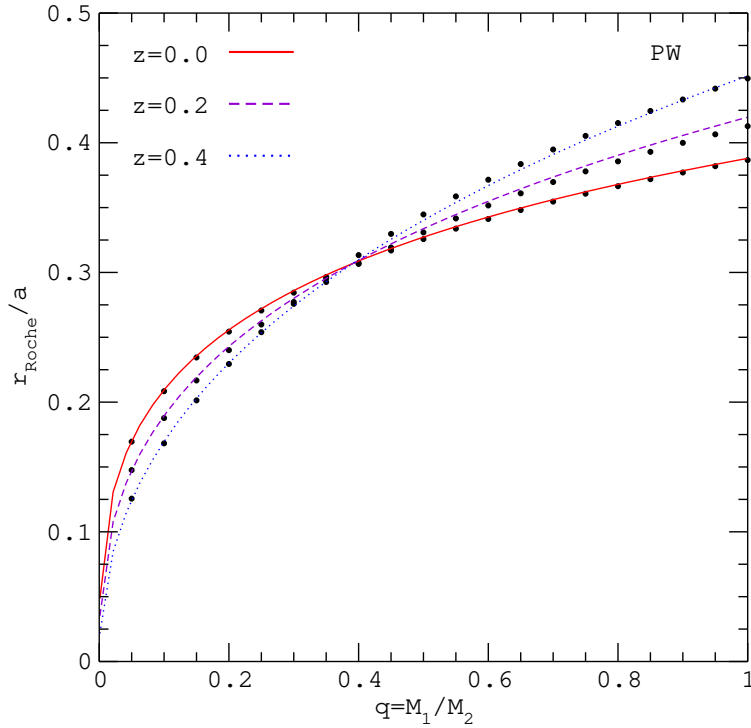


Fig. 7.— The ratio r_{Roche}/a as a function of q and z for the Paczyński–Wiita potential. The results of numerical integration are shown by dots whereas the curves represent the approximation in equation (14).

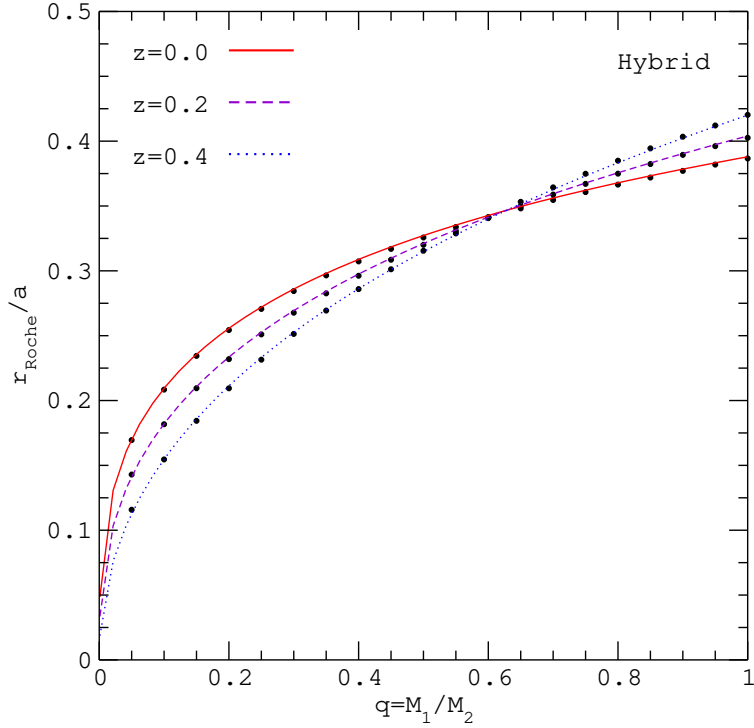


Fig. 8.— The ratio r_{Roche}/a as a function of q and z for the hybrid potential. The results of numerical integration are represented by dots whereas the curves represent the approximations in equation (14).

5.4. Evolution equations

The energy of a binary system is carried away through its gravity wave luminosity

$$L_{GW} = \frac{1}{5} \langle \ddot{\mathbb{F}}_{jk} \ddot{\mathbb{F}}_{jk} \rangle = \frac{32}{5} a^4 \mu^2 \omega^6. \quad (31)$$

Simultaneously, its angular momentum diminishes at the rate given by

$$\left(\dot{J}_{GW} \right)_i = \frac{2}{5} \epsilon_{ijk} \langle \ddot{\mathbb{F}}_{jm} \ddot{\mathbb{F}}_{km} \rangle = \frac{32}{5} a^4 \mu^2 \omega^5. \quad (32)$$

We note that these expressions do not depend on the form of the gravitational potential involved (i.e. Newtonian, Paczyński-Wiita, or our hybrid potential). The only assumptions that are made are weak gravitational field (linearized gravity) and slowly evolving circular orbits (a and angular frequency ω do not change significantly over a single period).

For the hybrid potential in equation (21), the energy of a binary system in a circular orbit is

$$E = \frac{a\mu M}{2(a - \zeta(q)r_G)^2} - \frac{\mu M}{a - \zeta(q)r_G}. \quad (33)$$

In the absence of mass transfer, this expression can be used to find the evolution of the system with time. As the separation a is decreases due to the emission of gravitational waves, the change in energy with time from equation (31) is given by

$$\dot{E} = \frac{\mu M}{2} \frac{a - 3\zeta(q)r_G}{(a - \zeta(q)r_G)^3} \dot{a} = -\frac{32}{5} \mu^2 M^3 \frac{a}{(a - \zeta(q)r_G)^6}. \quad (34)$$

The orbital angular momentum of a binary system with angular frequency ω , separation a , and reduced mass μ is $J = a^2 \mu \omega$. With the hybrid potential ϕ_H , the orbital angular frequency ω is given by equation (27). The orbital angular momentum will change in time because of gravitational radiation reaction. If mass transfer occurs, we will assume it conservative so that no further change to the orbital angular momentum occurs. Mass transfer, however, will result in a change in the mass ratio q . In response to radiation reaction and mass transfer, the change in the angular momentum can be written as

$$\dot{J} = \frac{d}{dt} \left[\frac{\mu a^{3/2} M^{1/2}}{a - \zeta(q)r_G} \right] = J \left\{ \left[\frac{1-q}{1+q} + \frac{r_G q \zeta'(q)}{a - \zeta(q)r_G} \right] \frac{\dot{q}}{q} + \frac{a - 3\zeta(q)r_G}{2(a - \zeta(q)r_G)} \frac{\dot{a}}{a} \right\}, \quad (35)$$

where we have used

$$\dot{A} \equiv \frac{d}{dt} A, \quad A' \equiv \frac{d}{dq} A, \quad \text{and} \quad \frac{d\mu}{\mu} = \frac{1-q}{1+q} \frac{dq}{q}, \quad (36)$$

for A any function of q and/or t . We recognize this as the pseudo-GR version of equation (2). The rate of angular momentum loss is given by equation (32), which we denote as \dot{J}_{GW} . This can be written as

$$\left[\frac{1-q}{1+q} + \frac{r_G q \zeta'(q)}{a - \zeta(q)r_G} \right] \frac{\dot{q}}{q} + \frac{a - 3\zeta(q)r_G}{2(a - \zeta(q)r_G)} \frac{\dot{a}}{a} = -\frac{\dot{J}_{GW}}{J} = -\frac{32}{5} M^2 \frac{\mu(t)}{(a(t) - \zeta(q)r_G)^4}. \quad (37)$$

In the absence of mass transfer, $\dot{q}(t) = \dot{\mu}(t) = 0$, whence

$$\dot{a} = -\frac{64}{5} \frac{a(t)}{a(t) - 3\zeta(q)r_G} \frac{M^2 \mu}{(a(t) - \zeta(q)r_G)^3}, \quad (38)$$

shows the orbital decay.

In the event of stable mass transfer, the radius of the lighter star is pinned to its effective Roche lobe radius, $R_1(t) = r_{Roche}(t)$. The time evolutions of R_1 and r_{Roche} are then governed by $q(t)$ and $a(t)$ which, combined with equation (13) gives the equivalent of equation (3):

$$\frac{\dot{r}_{Roche}}{r_{Roche}} = \left(1 + \frac{a}{C(q,z)} \frac{\partial C(q,z)}{\partial z} \frac{\partial z}{\partial a} \right) \frac{\dot{a}}{a} + \left(\frac{q}{Q(q)} \frac{\partial Q(q)}{\partial q} + \frac{q}{C(q,z)} \frac{\partial C(q,z)}{\partial q} \right) \frac{\dot{q}}{q}. \quad (39)$$

Utilizing the explicit dependences on q and z in equations (13) and (15), the derivatives needed above are easily evaluated. Explicitly,

$$\frac{\partial \ln Q(q)}{\partial \ln q} = \frac{2 \ln(1 + q^{1/3}) - (1 + q^{-1/3})^{-1}}{3[\beta_Q q^{2/3} + \ln(1 + q^{1/3})]}, \quad (40)$$

$$\frac{\partial C(q, z)}{\partial q} = \frac{\alpha_C}{5} \frac{z}{q^{4/5}}, \quad \text{and} \quad \frac{\partial C(q, z)}{\partial z} = \alpha_C q^{1/5} - \beta_C. \quad (41)$$

Equations (39) and (4) yield an expression analogous to equation (6):

$$\frac{\dot{q}}{q} = \frac{1 - \frac{\partial \ln C(q, z)}{\partial \ln z}}{\frac{\alpha}{1+q} - \frac{qQ'(q)}{Q(q)} - \frac{\partial \ln C(q, z)}{\partial \ln q}} \cdot \frac{\dot{a}}{a} \equiv \Upsilon(a, q) \frac{\dot{a}}{a}, \quad (42)$$

with

$$\begin{aligned} \Upsilon(a, q) \equiv & \left[\left(1 + z(\alpha_C q^{1/5} - \beta_C) \right) \right. \\ & \left. \times \left(\frac{\alpha(q, M)}{1+q} - \frac{2 \ln(1 + q^{1/3}) - (1 + q^{-1/3})^{-1}}{3[\beta_Q q^{2/3} + \ln(1 + q^{1/3})]} \right) - \frac{\alpha_C}{5} z q^{1/5} \right]^{-1}. \end{aligned} \quad (43)$$

Equation (37) allows us to separate the time derivatives of a and q to form the coupled equations

$$\frac{da(t)}{dt} = -\frac{32}{5} \frac{M^3}{a^3} \frac{1}{(1 - \zeta(q)z)^4} \frac{q}{(1+q)^2} \frac{1}{\left[\frac{1-q}{1+q} + \frac{zq\zeta'(q)}{1-\zeta(q)z} \right]} \Upsilon(a, q) + \frac{1 - 3\zeta(q)z}{2(1 - \zeta(q)z)} \quad (44)$$

and

$$\frac{dq(t)}{dt} = -\frac{32}{5} \frac{M^3}{a^4} \frac{1}{(1 - \zeta(q)z)^4} \frac{q^2}{(1+q)^2} \frac{\Upsilon(a, q)}{\left[\frac{1-q}{1+q} + \frac{zq\zeta'(q)}{1-\zeta(q)z} \right]} \Upsilon(a, q) + \frac{1 - 3\zeta(q)z}{2(1 - \zeta(q)z)}. \quad (45)$$

Note that in the absence of mass transfer ($\Upsilon(a, q) = 0$), equation (44) reduces to equation (38), and equation (45) yields $\dot{q}(t) = \dot{a}(t) = 0$. We note that the relativistic modifications complicate the evolution equations, but they do not qualitatively alter them.

6. Conditions for stable mass transfer

During the early stages of binary evolution, mass transfer is negligible and the orbital evolution is independent of the EOS. However, as the two objects approach each other, the Roche lobe radius shrinks until it becomes equal to the stellar radius R_1 . At this time, the lighter companion overfills its Roche lobe and mass transfer becomes possible. However, it is not guaranteed that mass transfer will be stable. As shown in §2, the condition for stable mass transfer is equation (10). If this condition is satisfied, mass transfer proceeds smoothly. If this condition is violated, mass transfer either terminates or grows uncontrollably since the star's radius increases faster than the Roche lobe radius. The restrictions imposed by equation (10) can be shown graphically for each choice of the gravitational potential and EOS. However, it is useful to examine some limiting situations with

a somewhat simpler analytic expression for $Q(q)$, derived by Kopal (1959), so that a qualitative interpretation can be made. To begin with, we neglect effects of relativity so that $z = 0$. In this case, the a dependence in Υ can be ignored. Using the simple expression

$$Q(q) = 0.46224 \left(\frac{q}{1+q} \right)^{1/3}, \quad (46)$$

which Kopal (1959) found to be a good approximation for $q < 0.8$, we obtain the approximate relation

$$\Upsilon(q) \simeq \frac{1+q}{\alpha - 1/3}. \quad (47)$$

For realistic neutron star or strange quark matter equations of state, $\alpha \leq 1/3$, so that Υ is negative as inferred in §2. In the case of a more detailed Roche lobe fit (like equation (13)), the limit to α can be somewhat smaller, which sometimes precludes very low mass strange quark stars from continuously transferring its mass in a stable fashion onto its companion.

In the Newtonian case, equation (10) now becomes

$$\Upsilon(q) < -\frac{1}{2} \frac{1+q}{1-q}. \quad (48)$$

Utilizing equations (47) and (48) turns the condition in equation (10) into

$$q < \frac{\alpha(M_1)}{2} + \frac{5}{6}, \quad \text{or} \quad \alpha(M_1) > 2q - \frac{5}{3}. \quad (49)$$

By selecting a fixed value for q , we can use this simple formula to find the range of masses for which a given equation of state allows for stable mass transfer to occur. In Figure 1, we designate with horizontal lines three values for q that are of special interest. For $q = 0$, corresponding to a heavy binary partner or a small M_1 , we obtain a line with $\alpha_0 = -5/3$. The equal mass $q = 1$ case is denoted with $\alpha_1 = 1/3$ in this figure, and the case $q = 0.5$ (often used in numerical evolutions in later sections) with $\alpha_{0.5} = -2/3$. We note that for mass transfer to be stable, the actual $\alpha(M_1)$ has to be greater than these values. In general, this forbids stable mass transfer for the $q = 1$ case even for the strange quark matter EOS, except in the $M_1 \rightarrow 0$ limit. Generally, stable mass transfer will be possible for normal EOS's when q is farther from unity than for strange quark mass stars. The limit for stable mass transfer imposed by equation (10) is shown schematically by the dashed curves for normal and SQM stars in Figure 9. We note that since the EOS parameter α becomes very negative for normal stars with low mass (see Figure 1), stable mass transfer eventually becomes impossible. This occurs for M_1 slightly larger than $M_{min} \simeq 0.09 M_\odot$, the minimum stable neutron star mass. This lower mass restriction, however, does not exist in the case of SQM stars.

The assumption of quasi-circular evolution in the pseudo-GR potential cannot be applied beyond the ISCO, the point of gravitational instability after which direct plunge onto the heavier companion is inevitable. Although mass transfer might ultimately ensue during the plunge, our

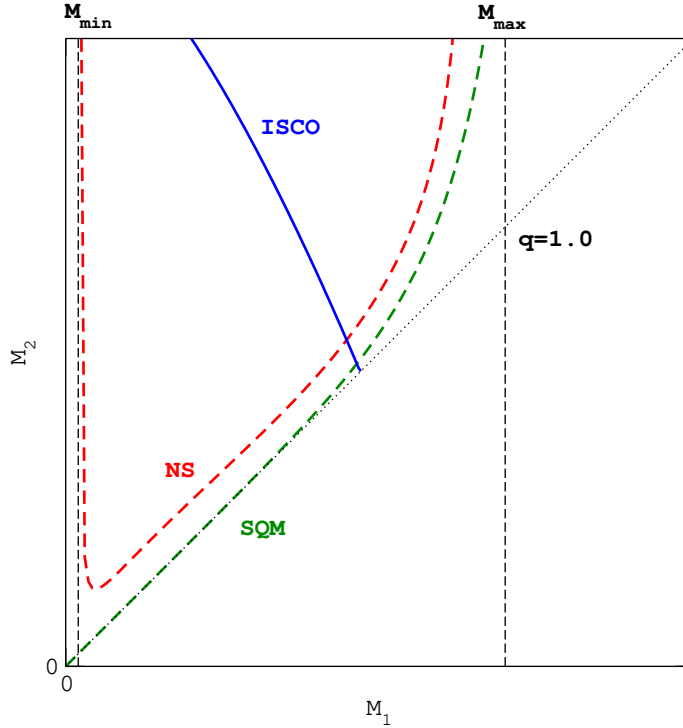


Fig. 9.— The limiting condition, that is, the lower mass limit to M_2 , for stable mass transfer is indicated by a dashed curve for the neutron star (NS) and strange quark matter star (SQM) cases. The solid curve shows the upper mass boundary for mass transfer beginning outside the ISCO. Other lines show the condition $q = 1.0$ and the maximum and minimum neutron star masses, M_{max} and M_{min} , respectively.

analysis is not trustworthy should mass transfer begin after the ISCO is reached. This establishes the limiting condition

$$R_1(M_1) = r_{ISCO} Q(q) C(q, \tilde{z}), \quad (50)$$

with $\tilde{z} = 2M/r_{ISCO}$, which can be phrased as a constraint in terms of M and q , or, alternatively, in terms of M_1 and M_2 . We utilize this condition for all potentials, despite the fact that the Newtonian potential does not predict an ISCO and the PW potential is deeper than the 2PN potential. The solid curve in Figure 9 shows, schematically, the limit dictated by equation (50): stable mass transfer occurs outside the ISCO for (M_1, M_2) values below this curve. For sufficiently large M_2 , or for $M_1 \simeq M_{max}$, both normal and self-bound stars are unable to transfer mass in a stable fashion within the ISCO limitation. From Figure 9, we infer that there exists a window in the M_1 – M_2 plane in which a merging binary system could evolve with stable and continuous mass transfer.

We now combine equations (10) and (50) with the results for all four potentials and for all six

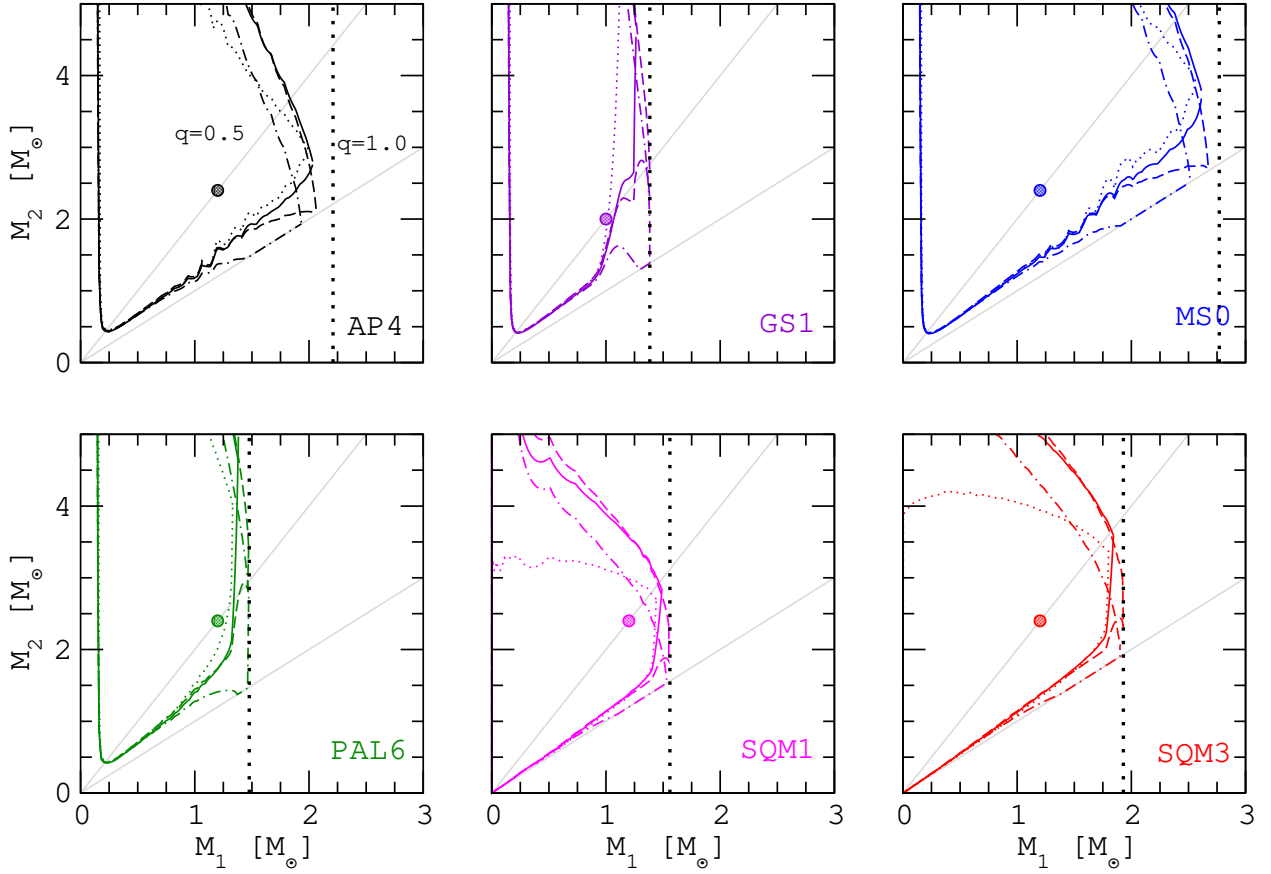


Fig. 10.— Limiting masses for stable mass transfer combining equations (10) and (50) for several equations of state and for the 2PN, hybrid pseudo-GR, Paczyński-Witta and Newtonian potentials, denoted by solid, dashed, dot-dashed and dotted curves, respectively. Filled circles indicate the masses employed in simulations discussed in §7. Two additional lines that correspond to $q = 1.0$ (equal mass case) and $q = 0.5$ (used in our evolutions) are shown.

equations of state that we have used (see Table 1 for notation and references). The ensuing results are shown in Figure 10. The qualitative picture of our simple analysis summarized in Figure 9 is not modified, only the quantitative details change. As in Figure 9, we find regions in the M_1 - M_2 plane for all four EOS's for which stable mass transfer is possible. In the next section, we discuss the evolution of merging binaries that undergo stable mass transfer.

7. Results of model evolutions

The numerical integration of the set of coupled differential equations in equations (8) and (9) were performed using a fourth order Runge-Kutta algorithm. The drastically different $\alpha(M)$

functions for normal and strange quark matter stars produce rather different behaviors after stable mass transfer begins. As a result, gravity wave emissions from these two types of mergers also differ. To underscore this, we will calculate the scalar gravitational polarization amplitude

$$h_+(t) = \frac{4}{r} \frac{M^2}{a} \frac{q}{(1+q)^2} \cos 2\omega(t-r), \quad (51)$$

where r is the distance from the binary system to the observer. The observed frequency of the emitted gravitational waves will be $2 \times 10^5 \omega/\pi$ Hz.

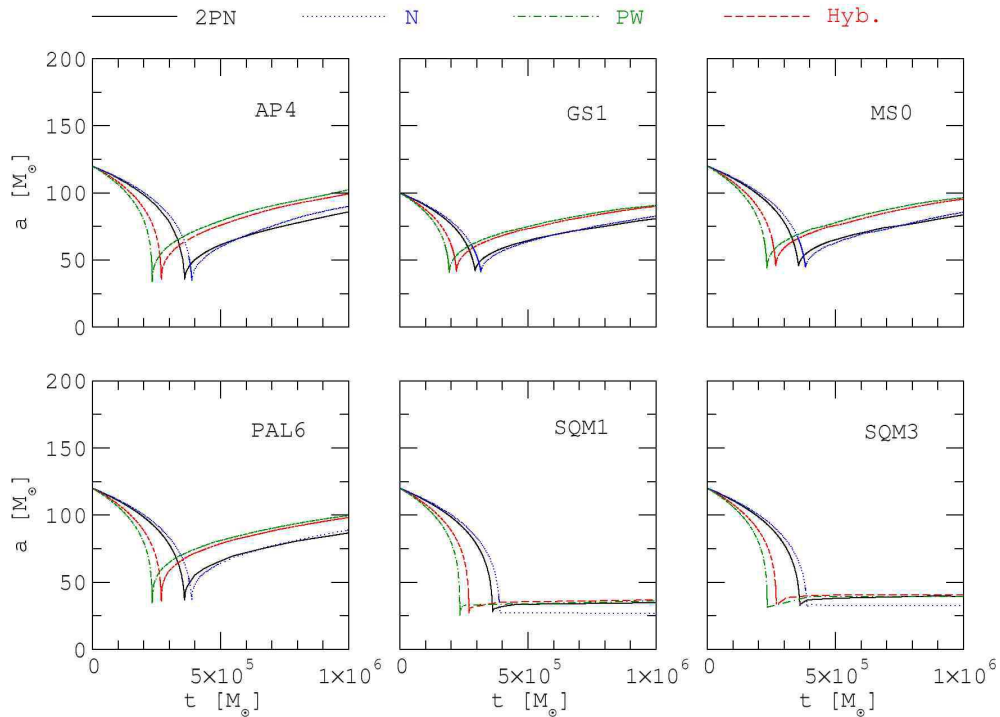


Fig. 11.— Evolution of the semimajor axis a ($1 M_\odot = 1.475$ km, $1 M_\odot = 4.92 \times 10^{-6}$ s) for the six EOS’s of Table 1. Line designations are as in Figure 10.

Figures 11–14 compare the mergers of normal and self-bound stars with a BH as described by equations (44) and (45). For these examples, the initial neutron star mass was taken to be $1.2 M_\odot$ in all cases except that of EOS GS1, for which the initial neutron star mass was taken to be $1.0 M_\odot$. In all cases, the initial mass ratio was $q = 0.5$, which guarantees that an epoch of stable mass transfer results. We are primarily interested in detailing the effects of stable mass transfer, so we do not consider cases in which tidal disruption occurs within the ISCO. For each EOS, evolutions were generated for the various gravitational potentials considered in this paper: Newtonian, second

order post-Newtonian, and the two pseudo-GR potentials. Inspiral is characterized by increases in the orbital frequency ω and scalar gravitational polarization amplitude h_+ , a decrease in orbital separation a , and a fixed q . Stable mass transfer ensues at the “kinks” visible in the evolution of these quantities. Within each class of EOS, i.e., normal and self-bound stars, variations in the EOS only qualitatively alter the results. During stable mass transfer, the decrease in orbital separation and rise in frequency and waveform amplitudes are reversed. The major effect of incorporating general relativistic corrections to the potential is to speed up the evolution relative to the Newtonian case. Stable mass transfer thus begins earlier in these cases. GR corrections also result in a somewhat larger value for the orbital separation following the onset of mass transfer.

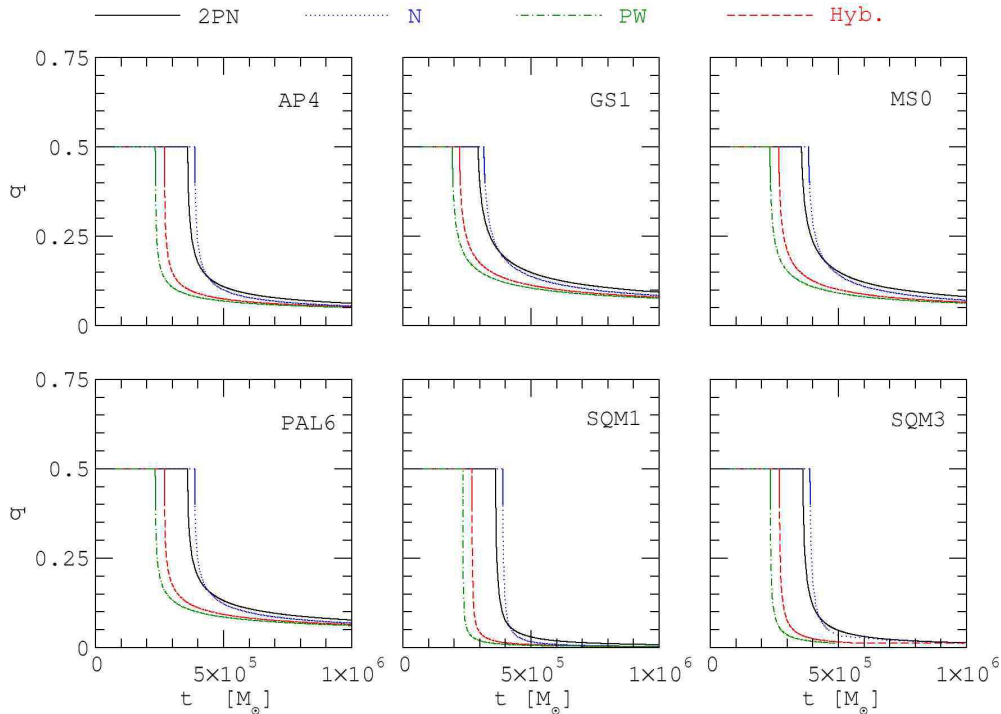


Fig. 12.— The same as Figure 11, but for the mass ratio q .

Large differences are apparent between the evolutions of the normal and self-bound cases.

1. The orbital separation $a(t)$ increases after mass transfer begins in the normal neutron star case, but quickly saturates in the self-bound case;
2. Reflecting the behavior of a , following the onset of stable mass transfer, the orbital angular frequency $\omega(t)$ continuously decreases in the normal case, but quickly achieves a relatively con-

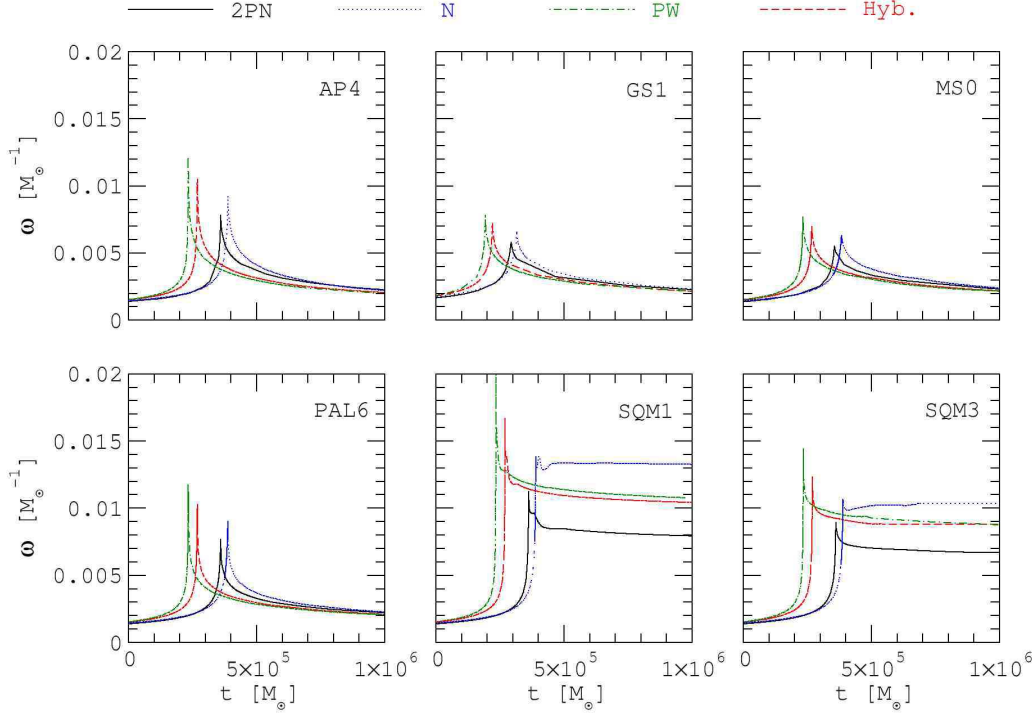


Fig. 13.— The same as Figure 11, but for the angular frequency ω . Note that the observed gravitational wave frequency is ω/π .

stant value in the self-bound case. A comparison of the evolution of ω for different equations of state is displayed in Figure 15 for the 2PN case, in which the zeros of time have been adjusted so that the onset of mass transfer is simultaneous. Also included in this figure are results for a polytropic equation of state $P = K\rho^\Gamma$ with $K = 0.0445c^2/\rho_n$, $\rho_n = 2.3 \times 10^{14} \text{ g cm}^{-3}$, and $\Gamma = 2$, which yields a radius of $\simeq 20.4 \text{ km}$ for the maximum mass star of $1.2M_\odot$. For the polytropic equation of state, $\alpha \rightarrow 0$ as $M \rightarrow 0$. Relatively large differences exist among the SQM star cases compared to the normal neutron star cases.

3. In the normal neutron star case, the mass M_1 approaches about $0.16 M_\odot$. Eventually, stable mass transfer terminates when α becomes too negative. Further evolution cannot be followed realistically with our model, but what apparently occurs is that the stellar radius now increases faster than the Roche lobe radius, indicating a catastrophic evaporation of mass from the neutron star. Since this occurs so closely to the neutron star minimum mass, about $0.09 M_\odot$ (this is independent of the supra-nuclear EOS), this evaporation is quickly followed by the decompression of the remaining neutron star (Colpi et al. 1993). In contrast, the mass of the

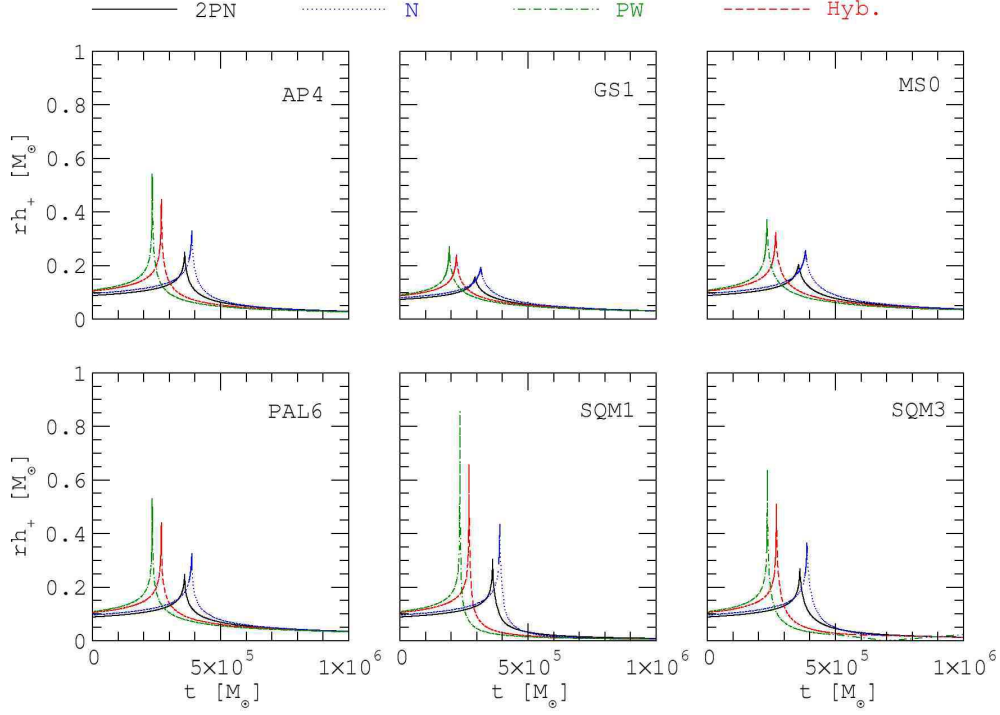


Fig. 14.— The same as Figure 11, but for the amplitude of the gravitational stress $|h_+|$ multiplied by the distance r .

self-bound star dwindles to extremely small values. In this case, the minimum mass limit is that of a strange quark nugget, determined in part by surface and Coulomb effects.

4. The envelope of the gravitational waveform amplitude $|h_+(t)|$ follows the behavior of q and a . In the normal neutron star case, the amplitude decreases steadily until stable mass transfer terminates. Following an initially rapid decrease, the amplitude decreases very slowly with time and continues indefinitely in the quark star case.

The evolution during the stable mass transfer phase can be qualitatively understood. The large differences observed between the strange quark star and the normal star cases arise as a result of the differing behaviors of the $\alpha(M_1)$ function in the limit of small M_1 . For the SQM case, $\alpha(M_1 \rightarrow 0) = 1/3$, whereas in the normal star case, it becomes increasingly negative. From equation (43), Υ quickly increases and tends to infinity for small q in the SQM case, so that $\dot{a} \rightarrow 0$ and a quickly stabilizes at a fixed value not much different than its value when stable mass transfer begins. However, in the normal star case, Υ steadily decreases, so that the denominators

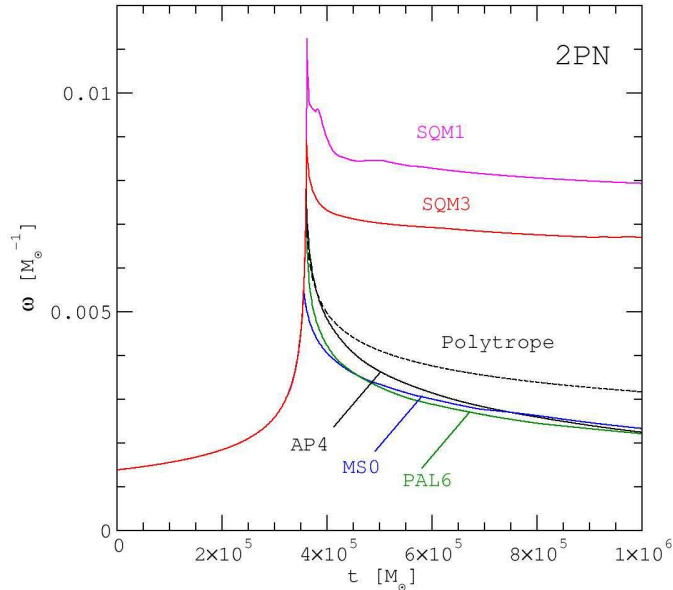


Fig. 15.— The evolution of ω for different equations of state for the Newtonian case, with the zeros of time adjusted so that the onset of mass transfer is simultaneous.

in equations (44) and (45) tend to zero as q decreases. Stable mass transfer terminates when the denominator vanishes, and formally \dot{q} and \dot{a} tend to infinity. However, the temporal evolution is speeded up so that both a and q reach particular final values in a finite time as shown in Figure (16). Mass continues to be lost from the neutron star, but now in a catastrophic, unstable, fashion because the stellar radius is expanding faster than the Roche lobe. When the star’s mass reaches M_{min} , the star essentially explodes as it becomes gravitationally unbound. The decompressing matter can then be expected to achieve relatively large velocities, possibly exceeding escape velocity from the system.

We can analytically examine the evolution in the normal star case by making a few simplifying approximations. First, we note that α diverges as the minimum stable neutron star mass, M_{min} , is approached. A useful approximation, valid for small M_1 , is

$$\alpha \approx -\frac{\alpha_0}{M_1 - M_{min}}, \quad (52)$$

where $\alpha_0 \simeq 0.089$ and $M_{min} \approx 0.09 M_\odot$. Using the Kopal approximation for $Q(q)$, equation (46),

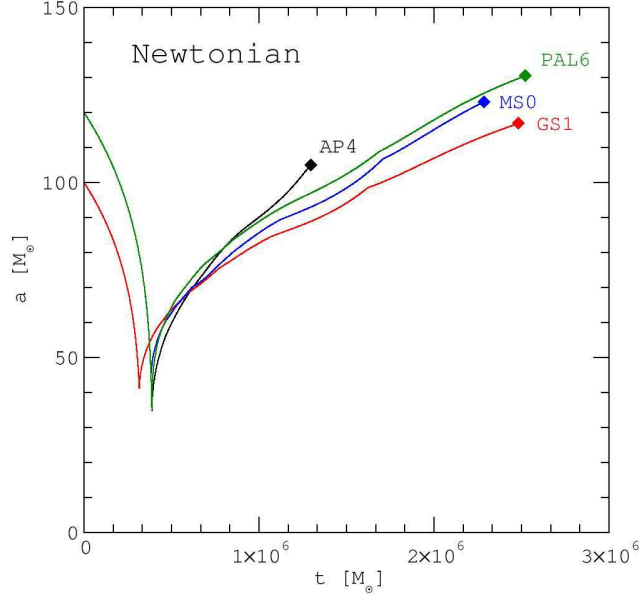


Fig. 16.— The evolution of the semimajor axis $a(t)$ for the Newtonian case, followed up to the end of stable mass transfer (indicated by filled diamonds), for the neutron star EOS’s AP4, PAL6, MS0 and GS1.

stable mass transfer terminates when

$$\alpha_f = 2q_f - \frac{5}{3} = -\frac{\alpha_0(1+q_f)}{q_f(M - M_{min}) - M_{min}}. \quad (53)$$

This suggests, for our standard case $M = 3.6 M_\odot$, that $\alpha_f \simeq -1.59$ and $q_f \simeq 0.04$, independently of the EOS. These values are close to those obtained in the numerical integrations. Furthermore, if equation (52) is also utilized, one can analytically integrate equation (42) to find

$$\frac{a}{a_f} \simeq \left(\frac{q_f}{q} \frac{1+q}{1+q_f} \right)^{1/3} \left(\frac{1+q_f}{1+q} \frac{\alpha}{\alpha_f} \right)^{\alpha_0/M_{min}}. \quad (54)$$

Although equation (52) is not valid for large values of M_1 , using that relation results in an estimate for our standard case that $a/a_f \simeq 0.21$, where a refers to the orbital separation when mass transfer begins. For comparison, Figure (16) indicates that a/a_f is actually in the range of 0.25–0.33. There is no simple way to estimate the duration of stable mass transfer, but figure (16) indicates it is of order $1 - 2 \times 10^6 M_\odot$ or about 5–10 seconds.

Similarly, we can analytically express the evolution of an SQM star during stable mass transfer

using the Kopal approximation, leading to

$$\begin{aligned}\dot{a} &= -\frac{32}{5} \left(\frac{M}{a}\right)^3 \frac{q}{(1+q)^2} \left(\frac{\alpha - 1/3}{\alpha/2 + 5/6 - q}\right), \\ \dot{q} &= -\frac{32}{5} \frac{M^3}{a^4} \frac{q^2}{1+q} \left(\frac{1}{\alpha/2 + 5/6 - q}\right).\end{aligned}\quad (55)$$

Since $\alpha = 1/3$ for moderate to small SQM star masses, we may assume a is approximately constant and equal to the value at which mass transfer begins. The equation for \dot{q} is then integrated to yield

$$\frac{\Delta t}{M} \simeq \frac{5}{32} \left(\frac{a}{M}\right)^4 \left(\frac{1}{q_f} + q_f - \frac{1}{q} - q\right), \quad (56)$$

where q_f is the value of q achieved for a time Δt after the stable mass transfer begins. Since the gravitational wave amplitude h_+ varies as $q/(1+q)^2$, as seen from equation (51), we expect this amplitude to decrease with time as t^{-1} , for an indefinite period of time.

However, how small can an SQM star become before the bulk EOS for SQM is inadequate? The bulk EOS is valid for an infinitely large system. As the strange quark star becomes small, Coulomb and surface effects become increasingly important. As shown by Farhi & Jaffe (1984), the bulk EOS is accurate only for values of the total baryon number $A = (N_u + N_d + N_s)/3 > 10^7$, which in our case translates to a value for $q_f \approx 2 \times 10^{-51}$. Obviously, $q \gg q_f$, so from equation (56) one finds $\Delta t \approx 10^{41}$ yr. Therefore the final disruption or merger of the strange quark matter star could never be observed.

One way to gauge the effects of different gravitational potentials is to compare the orbital evolution during inspiral. In order of relative gravity strengths, or attractiveness, we note the potential ordering Newtonian, 2 PN, hybrid and PW from Figures 11–14. The time elapsed during inspiral can be found by integrating equation (38), which results in

$$\begin{aligned}(a_{fin}^4 - a_{ini}^4) - 8\zeta(q)r_G(a_{fin}^3 - a_{ini}^3) + 24(\zeta(q)r_G)^2(a_{fin}^2 - a_{ini}^2) \\ - 40(\zeta(q)r_G)^3(a_{fin} - a_{ini}) + 12(\zeta(q)r_G)^4 \ln(a_{fin}/a_{ini}) = -\frac{256}{5}\mu M^2(t_{fin} - t_{ini}),\end{aligned}\quad (57)$$

where the initial radial separation and time are a_{ini} and t_{ini} , respectively, and the final separation and time (a_{fin} and t_{fin} , respectively) are chosen at the moment when mass transfer begins. The difference in the timescales between two potentials, for example, Newtonian and PW, can be established by differencing equation (57) for the two cases. However, although a_{ini} and t_{ini} can be taken as the same for the two cases, the two values of a_{fin} will be slightly different. Nevertheless, to lowest order this difference can be neglected and the difference $\Delta t = t_{fin,N} - t_{fin,PW}$ in evolution times for the two cases can be expressed as an expansion in the small quantity $\zeta(q)r_G$:

$$\frac{\Delta t}{M} \simeq \frac{5}{16} \frac{\zeta(q)r_g(1+q)^2}{q} \left(\frac{a_{fin}^3 - a_{ini}^3}{M^3}\right) + \mathcal{O}[(\zeta(q)r_G)^2]. \quad (58)$$

For our simulations, $M = 3.6 M_\odot$, $t_{ini} = 0$ and $a_{ini} = 120 M_\odot$, whence $\Delta t \simeq 1.5 \times 10^5 M_\odot$. This agrees well with our numerical result.

8. Discussion

As discussed in Cutler & Flanagan (1994), careful analysis of the gravitational waveform during inspiral yields values for not only the chirp mass $M_{chirp} = (M_1 M_2)^{3/5} / M^{1/5}$, but for also the reduced mass $M_1 M_2 / M$, so that both M_1 and M_2 can be found. Thus, observation of stable mass transfer effects in the gravitational wave signal will allow several details about neutron star structure to be discerned, including several features of the underlying EOS. For example,

1. The condition $r_{Roche} = R_1$ at the onset of mass transfer will allow a direct estimation of R_1 as a at that point is determined by M and ω , $a = M^{1/3} / \omega^{2/3}$. For example, in the Newtonian case, using the Kopal relation for Q , equation (46), this relation predicts that $\omega R_1 = 0.46^{3/2} M_1^{1/2}$. Thus a point (M_1, R_1) on the mass-radius diagram can be estimated. The effects of variations due to neutron star radii are less subtle for stable mass transfer than those which influence the inspiralling gravitational waveform (Faber et al. 2002).
2. Similarly, the condition $r_{Roche,f} = R_{1f}$ at the end of stable mass transfer yields a relation between M_{1f} and R_{1f} , where the subscript f refers to the final values indicating the end of stable mass transfer.
3. The ratio of the gravitational wave amplitudes h_+ at its peak and at the end of stable mass transfer h_{+f} , together with the ratio ω / ω_f , then can yield a value for the ratio R_1 / R_{1f} . Since R_1 has already been found, it is then feasible to estimate both R_{1f} and M_{1f} separately, so a second mass-radius pair can be found. For example, if the simple Kopal formula is used for the Roche lobe geometry, one finds

$$\frac{R_1}{R_{1f}} = \left(\frac{h_+}{h_{+f}} \right)^{1/3} \left(\frac{\omega_f}{\omega} \right)^{8/9} \left(\frac{1+q}{1+q_f} \right)^{1/3}. \quad (59)$$

4. Moreover, the end of stable mass transfer establishes a value (α_f) for α there. If we again use the simple Kopal relation for the Roche lobe geometry, equation (46), we obtain $\alpha_f \simeq -5/3 + 2q_f$. For low-mass neutron stars, $M_1 < 0.4 M_\odot$, we have observed that equation (52) is valid. This equation is relatively independent of the high-density EOS because such low-mass stars are primarily composed of matter below the nuclear saturation density. If the value for α_f is consistent with q_f , it means that mass transfer was indeed conservative. If they are not consistent, it is still possible, in principle, to then deduce a value for M_a which can be used to revise the estimates for M_{1f} and R_{1f} accordingly.
5. The time elapsed between the onset of stable mass transfer and its termination depends in a complicated way on q, M, R_1 and $\alpha(M)$. Nevertheless, measurement of this time, assuming that q and M are already measured, and that R_1 can be estimated as indicated above, implies that the function α can be constrained.

6. Most importantly, the sharp contrast between the evolutions during stable mass transfer of a normal neutron star and a strange quark star should make these cases distinguishable even if other information concerning the values of q , M and R_1 is weak. This result is independent of the form of the gravitational potential or the nuclear or quark matter EOS employed. During the phase in which mass transfer is present a normal star outspirals in order to preserve the total angular momentum of the system until the minimum mass limit is reached. In contrast, a strange quark matter star hovers at approximately constant separation distance during mass transfer for a very long time.
7. In addition, for the case of strange quark matter stars, the differences in the height of the frequency peak and the plateau in the frequency values at later times are related to the differences in radii of the stars at these two epochs. It is, therefore, indirectly an indicator of the maximum mass of the star: the closer is the star's mass before mass transfer to the maximum mass, the greater is the difference between these frequency values, because the radius change will be larger. As shown in Figure 15, the SQM1 case has a larger drop in the frequency than the SQM3 case because $1.2 M_\odot$ is closer to the maximum mass for the SQM1 case. Information about the maximum mass could therefore be revealed by these merging systems. Together with radius information, the value of the maximum mass remains the most important unknown that could reveal the true equation of state at high densities.

Given that the peak frequency observed in the gravitational wave signal has such a prominent role in determining the stellar radius in the event of stable mass transfer, we summarize our results for the Newtonian case in Table 3. We also indicate the estimated peak frequency using the approximation of equation (46) for the Newtonian case. The inverse connection between the peak frequency and the radius is apparent.

Relation with other works

We can compare our results to hydrodynamical simulations, both Newtonian and pseudo-GR, that have been performed. Kluźniak & Lee (2002) reported a series of hydrodynamical simulations of the mergers of a strange quark matter star with a more massive companion using the PW pseudo-GR potential. They found that the strange quark star plunged for any choice of masses in the binary system. However, the six cases they studied would, by our analysis, either fall into the situation $R_1 < r_{Roche,ISCO}$, for which mass transfer would begin only after the SQM star is plunging, or are borderline cases. We can employ equation (50) to find restrictions analogous to the ones in Figure 10 for the cases studied in Kluźniak & Lee (2002). In Table 4, we list the computed Roche radius at the ISCO for the six cases presented in Kluźniak & Lee (2002) and compare it to the results given there.

From Table 4, we note that the three $q = 0.3$ cases fall into the class of configurations that lead to a plunge. For the remaining three cases, we would have predicted stable mass transfer

Table 3. The value of the angular frequency ω at its peak.

EOS	AP4	GS1	MS0	PAL6	SQM1	SQM3
$\omega_{\text{peak, 2PN}} [10^{-3} M_{\odot}^{-1}]$	9.20	6.54	6.28	9.02	13.83	10.65
$\omega_{\text{Eq. (46)}} [10^{-3} M_{\odot}^{-1}]$	9.25	6.56	6.32	9.13	13.79	10.78
R_1 [km]	11.4	13.5	14.7	11.5	8.7	10.3

Note. — Comparison of the angular frequencies at the beginning of mass transfer. In the first line, we show results for the angular frequencies ω from our calculations in Figure 13. In the second line, we show ω as given by the Newtonian approximation utilizing equation (46). All cases were computed for $M_1 = 1.2 M_{\odot}$ and $M_2 = 2.4 M_{\odot}$, except GS1 for which $M_1 = 1.0 M_{\odot}$ and $M_2 = 2.0 M_{\odot}$. The corresponding radii R_1 at those masses are also shown.

Table 4. The mass transfer-ISCO restriction for Kluźniak & Lee (2002).

q	M_1/M_{\odot}	M/M_{\odot}	R_1 [km]	$R_{\text{Roche, ISCO}}$ [km]
0.5	1.5	4.5	9	8.43
0.3	1.5	6.5	9	10.17
0.5	2.0	6.0	12	11.25
0.3	2.0	8.67	12	13.57
0.5	2.5	7.5	15	14.05
0.3	2.5	10.83	15	16.96

and a relatively slower subsequent evolution. Nevertheless, all three of these cases are close to the borderline of the plunge regime and, although Kluźniak & Lee (2002) attribute this effect to properties of the strange quark star, it could well be that the plunge they observed is primarily a property of the PW pseudo-GR potential, which is somewhat stronger (deeper) than the 2PN potential we employed. The ISCO is closer in for the 2PN potential compared to the PW potential, as graphically illustrated in Figure 4.

As noted by Faber et al. (2002), compactness of the star might be recorded in the emerging gravitational radiation during inspiral. For the example of a polytropic EOS, the spectrum dE/df of gravitational waves depends on the ratio of the star’s mass and its radius M_1/R_1 . However, in our analysis, the height of the frequency peak just before mass transfer begins contains important information about the radius of the star R_1 that might be more accurate than that extracted from the inspiral waveform. Hence, conditional upon having information about M_1 and M_2 , the frequency of the emerging gravitational signal could be utilized to measure the star’s radius.

Several assumptions have been utilized in our simulations, including the conservation of the total mass and angular momentum (except for the angular momentum radiated in gravitational radiation) of the stars, and quasi-circular orbits. Conservation of mass and angular momentum of the stars could be modified by the formation of an accretion disc or by the ejection of mass from the system. In the absence of a violent tidal disruption, ejection of mass to infinity seems unlikely, but an accretion disc could form a reservoir that could modify the orbital evolution during stable mass transfer and the resulting gravity wave signal. Also, the assumption of circular orbits is not reliable near the ISCO, with moderate errors in the evaluation of the orbital phase (see Miller (2004b)). More accurate numerical work will be required to establish detailed waveforms for comparison to experiment, especially if stable mass transfer ensues near the ISCO.

Another assumption is that the ISCO marks a sharp cutoff outside of which stable mass transfer is assumed to be possible. Miller (2004a) argues that angular momentum loss to gravitational radiation is significant during the time interval necessary for mass transfer to ensue, so that the plunge of the stars actually starts well outside the ISCO. Using the Peter’s formula for angular momentum loss due to gravitational radiation, and assuming the Newtonian formula for orbital angular momentum, one can estimate $N(a_i)$, the number of orbits remaining until the ISCO is reached, as a function of the initial orbital separation a_i :

$$\begin{aligned} N(a_i) &= \int_{a_i}^{a_{ISCO}} \frac{1}{P(a)\dot{J}_{GW}(a)} \frac{dJ(a)}{da} da \\ &= \frac{(1+q)^2}{64\pi q} \left(\frac{a_{ISCO}}{M}\right)^{5/2} \left[\left(\frac{a_i}{a_{ISCO}}\right)^{5/2} - 1 \right] \simeq 0.92 \left[\left(\frac{a_i}{a_{ISCO}}\right)^{5/2} - 1 \right]. \end{aligned} \quad (60)$$

In the last line above, we used $M_1 = 1.2 M_\odot$ and $M_2 = 2.4 M_\odot$ and $a_{ISCO}/M \simeq 4.4$ as appropriate up to 2PN order. From equation (60), we find that for $a_i/a_{ISCO} = 1.1$ only 1/4 orbit remains until $a = a_{ISCO}$. If $a_i/a_{ISCO} = 1.5$, we find 5/4 orbits remain. The relevant timescales are determined by the orbital period, which is approximately $P = 0.7(a/a_{ISCO})^{3/2}$ ms for our conditions. Clearly,

mass transfer would have to occur relatively quickly for our scenario to be realized. Newtonian SPH hydrodynamical simulations, however, have indeed found that stable mass transfer can occur (see, *e.g.*, Rosswog & Speith (2004)).

Results using the Newtonian potential are suspect because the values of the angular frequency and separation near the onset of stable mass transfer imply orbital velocities in the range 0.5 to $0.6c$. (See Thorne (1973) for more elaboration on this problem.) Our results indicate, however, that the use of either of the two pseudo-GR potentials probably overestimates the strengthening of gravity due to GR. The results for the 2-PN case, in fact, are intermediate between the Newtonian and pseudo-GR cases and relatively close to the Newtonian results.

In this context, it is interesting to compare recent calculations of black hole-neutron star mergers performed by Rosswog & Speith (2004) and Rosswog (2005). In the former paper, Newtonian simulations are carried out, whereas in the latter paper the Newtonian potential is replaced by the Paczyński-Wiita potential. Episodic (stable) mass transfer is found in the Newtonian case whereas the use of the PW potential results in tidal disruption of the neutron star inside the ISCO (but accompanied by the ejection of a small-massed tidal tail). Our calculations indicate that the Paczyński-Wiita potential is too strong compared to the 2PN potential, which gives results closer to the Newtonian case. Also, the Paczyński-Wiita simulations of Rosswog (2005) only considered black hole masses greater than $14 M_{\odot}$, in which case we would not have expected stable mass transfer to take place in any event.

The argument of Miller (2004a) concerning the lack of time for mass transfer to stabilize the orbit of the merging binary is independent of whether the geometry considered is Newtonian or relativistic. Since the Newtonian simulations of Rosswog & Speith (2004) and others (*cf.*, Lee et al. (2001) and references therein) showed that stable mass transfer was nevertheless possible, it would be very interesting to see if stable mass transfer also occurs in hydrodynamic simulations that use a potential correct to 2PN together with smaller black hole masses.

9. Conclusions

We have extended Newtonian models of binary orbital evolution and Roche lobe geometry to second post-Newtonian order to examine the final stages of compact binary mergers in which the lighter star is a neutron star or a strange quark matter star. In our simulations, binary mergers can be categorized into two distinct classes, depending upon whether or not stable mass transfer occurs. We find that similar, non-negligible, regions in mass space ($M_1 - M_2$) allow for the possibility of stable mass transfer for both normal neutron stars and strange quark matter stars. Mass transfer is not expected to occur if (1) the binary mass ratio $q = M_1/M_2$ is too close to unity, or (2) the total mass of the system is too large ($M \gtrsim 10 M_{\odot}$). The limit on q for normal stars is $q \gtrsim 0.75$, but for strange quark matter stars it is $q \gtrsim 0.9$.

Binary mergers in which stable mass transfer is able to occur behave dramatically different

than those in which plunge occurs. Qualitatively, normal stars and SQM stars follow a similar evolution: stable mass transfer initiates a period of reverse, or outwards, spiralling, characterized by diminishing frequencies and gravitational wave amplitude, that has a duration of 5–10 s in the case of normal stars and lasts essentially forever in the case of SQM stars. In contrast, the gravitational wave emission of a plunge is characterized by a single burst of high-frequency radiation. These differences should be distinguishable from gravitational radiation observations.

In the case of stable mass transfer, large differences in the gravity wave signal following the onset of mass transfer between the cases of normal neutron stars and strange quark matter stars are expected. This signature may be unique in its ability to distinguish between these stellar models from astrophysical observations. Whereas normal neutron star evolutions will be characterized by rapidly diminishing frequencies, strange quark matter star evolutions will have a radiation frequency that reaches an asymptotic value. In addition, stable mass transfer from a normal neutron star will have a finite duration of order 5–10 s, concluding when the star expands quickly and overfills its Roche lobe when its mass decreases to about $0.16 M_{\odot}$, which will be quickly (of order a few ms) followed by the violent decompression of the star when it reaches its minimum mass (about $0.09 M_{\odot}$). In contrast, mass transfer should continue essentially forever in the case of an SQM star, with a gravitational wave amplitude that decreases with time as t^{-1} .

Several observational constraints become possible from mergers in which stable mass transfer occurs. Most important is the ability to distinguish between the star being normal or composed of strange quark matter. In either case, the possibility exists to extract the radius-mass relation. Not only will a distinct $M - R$ point be potentially measureable from a single system, corresponding to the onset of stable mass transfer, but in the case that the star is normal, an additional point is possible corresponding to the termination of stable mass transfer. The overall signal may also allow estimation of the function $\alpha(M) = d \ln r / d \ln M$ for intermediate masses. Moreover, observations of many different events will allow sampling of a corresponding number of $M - R$ points.

Research support of the U.S. Department of Energy under grant number DOE/DE-FG02-87ER-40317 for all authors and grant number DOE/DE-FG02-93ER-40756 for Madappa Prakash is gratefully acknowledged.

REFERENCES

- Alcock, C. & Olinto, A. 1988, *Ann. Rev. Nucl. Part. Sci.*, 38, 161
- Alford, M. 2001, *Ann. Rev. Nuc. Part. Sci.*, 51, 131
- Bejger, M., Gondek-Rosińska, D., Gourgoulhon, E., Haensel, P., Taniguchi, K., & Zdunik, J. L. 2005, *A&A*, 431, 297, [arXiv:astro-ph/0406234](https://arxiv.org/abs/astro-ph/0406234)
- Bethe, H. A. & Brown, G. E. 1998, *ApJ*, 506, 780

- Blanchet, L. 2002, *Living Rev. Relativity*, 5
- Blanchet, L. & Iyer, B. 2003, *Class. Quantum Grav.*, 20, 755
- Burgay, M., D’Amico, N., Possenti, A., Manchester, R., Lyne, A., Joshi, B., McLaughlin, M., Kramer, M., Sarkissian, J., Camilo, F., Kalogera, V., Kim, C., & Lorimer, D. 2003, *Nature*, 426, 531L
- Burrows, A. & Lattimer, J. M. 1986, *ApJ*, 307, 178
- Chau, W. Y. 1976, *Astrophys. Lett.*, 17, 119
- Clark, J. 1977a, *Astrophys. Lett.*, 18, 73
- Clark, J. P. A. 1977b, *Astrophys. Lett.*, 18, 73
- Colpi, M., Shapiro, S. L., & Teukolsky, S. A. 1993, *ApJ*, 414, 717
- Cutler, C. & Flanagan, E. E. 1994, *Phys. Rev. D*, 49, 2658
- Damour, T. & Schäfer, G. 1985, *Gen. Relativ. Gravit.*, 17, 879
- Davies, M. B., Levan, A. J., & King, A. R. 2005, *MNRAS*, 356, 54
- de Andrade, V. C., Blanchet, L., & Faye, G. 2001, *Class. Quantum Grav.*, 18, 753
- Eggleton, P. P. 1982, *ApJ*, 268, 368
- Eichler, D. and Livio, M., Piran, T., & Schramm, D. N. 1989, *Nature*, 340, 126
- Faber, J. A., Grandclement, P., Rasio, F. A., & Keisuke, T. 2002, *Phys. Rev. Lett.*, 89, 231102
- Farhi, E. & Jaffe, R. L. 1984, *Phys. Rev. D*, 30, 2379
- Finn, L. S. 2001, in *American Institute of Physics Conference Proceedings*, Vol. 575, *Astrophysical Sources for Ground-based Gravitational Wave Detectors*, ed. J. M. Centrella, American Institute of Physics (Melville, NY: American Institute of Physics), 92
- Jaranowski, P. & Krolak, A. 1992, *ApJ*, 394, 586
- Kalogera, V., Kim, C., Lorimer, D., Burgay, M., D’Amico, N., Possenti, A., Manchester, R., Lyne, A., Joshi, B., McLaughlin, M., Kramer, M., Sarkissian, J., & Camilo, F. 2004, *ApJ*, 601, L179
- Kluźniak, W. & Lee, W. H. 2002, *MNRAS*, 335, L29
- Kopal, Z. 1959, *Close Binary Systems* (New York: Wiley)
- Lattimer, J. & Prakash, M. 2001, *ApJ*, 550, 426

- Lattimer, J. & Schramm, D. 1976, *ApJ*, 210, 549
- Lattimer, J. M., Mackie, F., Ravenhall, D. G., & Schramm, D. N. 1977, *ApJ*, 213, 225
- Lee, W., Kluźniak, W., & Nix, J. 2001, *Acta Astronomica*, 51, 331
- Lyne, A., Burgay, M., Kramer, M., Possenti, A., Manchester, R., Camilo, F., McLaughlin, M., Lorimer, D., D’Amico, N., Joshi, B., Reynolds, J., & Freire, P. 2004, *Science*, 303, 1153
- Madsen, J. 1999, in *Lecture Notes in Physics*, Vol. 516, *Hadrons in Dense Matter and Hadrosynthesis*, ed. J. Cleymans (New York, Berlin, Heidelberg: Springer-Verlag GmbH), 162–203, [arXiv:astro-ph/9809032](#)
- . 2002, *J. Phys. G*, 28, 1737
- Meyer, B. S. 1989, *ApJ*, 343, 254
- Miller, M. 2004a, Submitted to *ApJ*, [arXiv:astro-ph/0505094](#)
- . 2004b, *Phys. Rev. D*, 69, 124013
- Paczyński, B. 1971, *ARA&A*, 9, 183
- Paczyński, B. & Wiita, P. J. 1980, *A&A*, 99, 23
- Portegies Zwart, S. F. 1998, *ApJ*, 503, 53
- Portegies Zwart, S. F. & Yungelson, L. R. 1998, *A&A*, 332, 173
- Prakash, M., Baron, E., & Prakash, M. 1990, *Physics Letters B*, 243, 175
- Prakash, M. & Lattimer, J. 2003, *Jl. of Phys. G: Nucl. Part. Phys.*, 30, S451
- Prakash, M., Lattimer, J. M., Pons, J. M., Steiner, A. W., & Reddy, S. 2000, *Lect. Notes Phys.*, 578, 364
- Prakash, M., Ratković, S., & Lattimer, J. M. 2004, *J.Phys. G*, 30, S1279, [arXiv:astro-ph/0403374](#)
- Ratković, S., Lattimer, J., & Prakash, M. 2005, Submitted to *ApJ*, [arXiv:astro-ph/0512133](#)
- Rosswog, S. 2005, [arXiv:astro-ph/0505007](#)
- Rosswog, S. & Speith, R. and Wynn, G. 2004, *MNRAS*, 351, 1121
- Shibata, M. 2005, To appear in *Phys. Rev. Lett.*, [arXiv:gr-qc/0504082](#)
- Shibata, M., Taniguchi, K., & Uryū, K. 2003, *Phys. Rev. D*, 68, 084020
- Shibata, M., Taniguchi, K., & Uryu, K. 2005, *Phys. Rev. D*, 71, 084021, [arXiv:gr-qc/0503119](#)

Thorne, K. S. 1973, in *Three Hundred Years of Gravitation*, ed. S. Hawking & W. Israel (Cambridge: Cambridge university Press)

Witten, E. 1984, *Phys. Rev. D*, 30, 272